STATISTICAL OPTIMIZATION OF PERVIOUS CONCRETE PAVEMENT CONTAINING FLY ASH AND ENGINEERED IRON OXIDE NANOPARTICLES FOR RUNOFF QUALITY AND QUANTITY CONTROLS

By

NATALIA ISABEL VÁZQUEZ RIVERA

A project report submitted in partial fulfillment of the requirements for the degree of
MASTER IN ENGINEERING
In
CIVIL ENGINEERING
(Environmental and Water Resources Engineering)
UNIVERSITY OF PUERTO RICO
MAYAGÜEZ CAMPUS
2014

Approved by:

_____	_____
Sangchul Hwang, PhD President, Graduate Committee	Date
_____	_____
Omar I Molina Bas, PhD Member, Graduate Committee	Date
_____	_____
Moses Bogere, PhD Member, Graduate Committee	Date
_____	_____
Paul Sundaram, PhD Representative of Graduate School	Date
_____	_____
Ismael Pagán Trinidad, MSCE Director, Department of Civil Engineering and Surveying	Date

Summary

Portland cement pervious concrete (PCPC) usage has increased due to its potential to reduce storm water runoff and related pollution. Partial Portland cement substitution by fly ash (FA) in concrete production has the advantages of reducing cost, carbon dioxide production associated with Portland cement production and burden of solid waste management. In this regard, a cementitious paste was characterized and a PCPC mixture was optimized by Response Surface Methodology. Also the PCPC was tested for phosphorus removal capacity.

As part of the characterization of cementitious paste, spread percentage and setting time were measured. The addition of engineered iron oxide nanoparticles coated with surfactant ($ENP_{Fe\text{-}surf}$) increased both the spread percentage and setting time. Also the $ENP_{Fe\text{-}surf}$ addition slightly increased weight gain when exposed to sulfuric acid, but slightly decreased weight loss when exposed to acetic acid. It is possible that $ENP_{Fe\text{-}surf}$ facilitates the production of calcium silicate hydrate (C-S-H gel), iron-substituted monosulfate hydrate, or iron-substituted ettringite. The specimens exposed to sulfuric acid had higher compressive strength values compared to those exposed to acetic acid for 90 days.

A two-level central composite factorial design was used to investigate the effects of water to powder ratio (W/P, 0.34-0.40), percentage of cement substitution by FA (FA/B, 0.1-0.4) and $ENP_{Fe\text{-}surf}$ to powder ratio (ENP/B, 0.03-0.05) on compressive strength, permeability, void content and hardened density of pervious concrete. Limestone gravels passing through 9.5-mm sieve but retained on 4.75-mm sieve were used. The results showed compressive strength, permeability, void content and hardened density in the ranges of 2.5-13.5 MPa, 5.3-17.4 mm/sec, 12-22 % and 2120-2360 kg/m^3, respectively. W/B and FA/B had significant impacts on all the

properties of PCPC studied, whereas ENP/B produced significance only for the compressive strength. Optimal region was found for the desired PC parameters at W/B 34%, FA/B 15% and ENP/B 5%.

The PCPC was capable of removing phosphorus by adsorption and/or precipitation. The PCPC specimens with $ENP_{Fe\text{-}surf}$ had greater removal capacity so it is believe that it facilitated phosphate removal. There was 7% and 10% difference between the first-order phosphorus removal constant obtained for PCPC specimens with or without $ENP_{Fe\text{-}surf}$. Similarly, there was between 6% to 10% difference for the Freundlich isotherm K_f coefficients obtained for control samples compared to the sample that had FA and $ENP_{Fe\text{-}surf}$ added. The dissolution of calcium hydroxide from PCPC was believed to facilitate phosphorus precipitation probably as amorphous calcium phosphorus or hydroxyapatite.

Fenton regeneration increased permeability of bioclogged PCPC specimens. $ENP_{Fe\text{-}surf}$ addition did not play a role in Fenton oxidation. Instead, iron species containing FA were believed to work as the iron catalyst for Fenton oxidation. Compressive strength was not negatively affected despite string oxidation reaction during Fenton regeneration.

Resumen

El uso de pavimentos de hormigón permeable (PCPC por sus siglas en inglés) ha aumentado debido a su potencial a reducir escorrentías y la contaminación relacionada a ella. La sustitución parcial del cemento Portland por cenizas volantes en la producción de hormigón tiene las ventajas de reducir costos, la producción de dióxido de carbono relacionado a la producción de cemento Portland y cargas al manejo de desperdicios sólidos. En este sentido una pasta cementicia fue caracterizada y una mezcla de PCPC fue optimizada por Metodología de Superficies de Respuestas (RSM). También se midió la capacidad de PCPC de remover fósforo.

El porcentaje de propagación y el tiempo de fraguado fueron medidos como parte de la caracterización de la pasta cementicia. La adición de nanopartículas de hierro oxidado recubiertas de surfactante ($ENP_{Fe\text{-}surf}$) aumento el porcentaje de propagación y el tiempo de fraguado. La adición de $ENP_{Fe\text{-}surf}$ también aumento ligeramente la ganancia de peso de las pasta al ser expuestas a ácido sulfúrico pero disminuyo ligeramente su peso al ser expuestas a ácido acético. Es posible que $ENP_{Fe\text{-}surf}$ facilite la producción del gel C-S-H, etringita (sustitución por hierro) y monosulfato hidratado (sustitución por hierro). Las especies expuestas a ácido sulfúrico obtuvieron valores en compresión mecánica en comparación con aquellas expuestas a ácido acético por 90 días.

Un diseño compuesto central de dos niveles fue usado para investigar los efectos que la razón agua a conglomerante (W/B, 0.34-0.40), cantidad de cemento sustituido por cenizas volantes (FA/B, 0.1-0.4) y cantidad de $ENP_{Fe\text{-}surf}$ añadida por cantidad de conglomerante (ENP/B, 0.03-0.05) tienen en compresión mecánica, permeabilidad, contenido de espacios libres y densidad. Gravilla de caliza que pasa a través del tamiz de 9.5 mm pero se retiene en el de 4.75

mm fue usada. Los resultados mostraron compresión mecánica, permeabilidad, contenido de espacios libres y densidad en los rangos de 2.5-13.5 MPa, 5.3-17.4 mm/s, 12-22% y 2120-2360 kg/m^3, respectivamente. Hubo un impacto significativo en todas las propiedades de PCPC estudiadas debido a W/B y FA/B, mientras que ENP/B produjeron un impacto significativo solo en la tensión mecánica. Una región con razones óptimas fueron encontradas para los parámetros deseados en W/B 0.34, FA/B 0.15 y ENP/B 0.05.

El PCPC es capaz de remover fosfato por adsorción y precipitación. Las especies de PCPC con $ENP_{Fe\text{-}surf}$ tuvieron una mayor capacidad de remoción por lo que se cree que facilitan la remoción de fosfato. Había una diferencia entre 10 y 13% entre las constantes de remoción de fosfato de primer orden obtenido por las especies con o sin $ENP_{Fe\text{-}surf}$. Similarmente había entre 6% y 10% de diferencia entre los coeficientes K_f de la isoterma de Freundlich comparando muestras de control con la muestra que contenía FA y $ENP_{Fe\text{-}surf}$. Se cree que la disolución de hidróxido de calcio de PCPC facilita la precipitación de fosfato probablemente como fosfato de calcio amorfo.

Regeneración Fenton aumenta la permeabilidad de muestras PCPC biobloqueadas. La adición de $ENP_{Fe\text{-}surf}$ no mostró importancia en la oxidación Fenton. En cambio se cree que las especies de hierro que se encuentran en las cenizas volantes sirvieron de catalizador para la oxidación Fenton. La compresión mecánica no fue afectada negativamente a pesar de fuerte reacción de oxidación durante la regeneración Fenton.

Acknowledgement

I wish to give thanks to a group of people. Without their guidance, encouragement, and contribution this research would not be the same.

First of to my adviser Dr. Sangchul Hwang, without whose attention, guidance, and assistance I would not be able to obtain my master's degree. To committee members and reviewers: Dr. Omar Molina, Dr. Moses Bogere, Ismael Pagán, for all their notes and advice.

My sincere appreciation is extended to AES Puerto Rico and Wi(PR)$_2$EM (NSF DMR-0934115) for financial support. To the engineers Victor Aviles and Ruben Segarra, from Essroc San Juan, for the chemical composition analysis of Portland cement and fly ash.

To my laboratory partners: Linoshka Soto, Margaret Hernandez, Keila Pagán, and Isomar Latorre for all their moral support, good laughs, each kind word and many coffee breaks. To Rene Santiago, Juliana St. John, Isaias Gustavo Torres for all their helping hands.

Last but not least, to my parents, Roberto Vazquez and Bertha Rivera, and my sister, Beatriz Vazquez for their unconditional love and support.

Table of Content

List of Figures

List of Tables

1. Introduction

As time passes by, more surfaces are becoming impervious. This prevents natural percolation of water through the soil and groundwater recharge and increases stormwater runoffs. Runoffs can cause flooding, soil erosion, and pollutant transport. Civil engineers use detention or retention ponds to reduce such negative impacts of stormwater runoffs. However, the technologies require a large amount of space that could potentially be developed for other purposes (Garber, 2010). Pervious or porous pavement is a greener approach to reduce stormwater runoffs (Scholz and Grabowiecki, 2007). Portland cement pervious concrete (PCPC) or enhanced porosity concrete pavement can reduce runoffs and the associated pollutants. It could also reduce, and in some case; even eliminate the necessity of detention or retention ponds (Garber, 2010). Portland cement pervious concrete is capable of reducing non-point source pollutants before they reach surface water, groundwater and wastewater treatment plants. It would benefit the environment and public health and reduce treatment costs.

Portland cement pervious concrete is a material that permits the percolation of water through its interconnected pores, which is capable of reducing runoffs and heat island effect and absorbing noise (ACI, 2010; Garber, 2010). Both water and air can enter its pores and saturate the soil underneath and feed groundwater. Portland cement pervious concrete is usually designed to have a void ratio from 15 to 35% and a permeability ranging between 1.4 to 12.3 mm/s (0.055 – 0.48 in/s) (ACI, 2010). It has a typical compressive strength ranging from 2.8 to 28 MPa (406 – 4060 psi), which limits its potential usage (ACI, 2010). In order for PCPC to be used for structural purposes it must have a minimum of 27 MPa (3920 psi) of compressive strength. Some researchers have proposed the use of PCPC to decrease or eliminate pollutants from runoff and

improve water quality (Huang et al., 2010). Also PCPC was proposed to use for agricultural activities and animal production facilities to reduce the adverse effect they have on water quality (Luck et al., 2008).

Portland cement pervious concrete is composed of Portland cement, air, water and coarse aggregate, but it can also include fine aggregate (for example, sand), fibers, mineral admixtures, and chemical admixtures. Mineral admixtures with pozzolanic activity, like silica fume and fly ash (FA), are powder materials that can react with calcium hydroxide in presence of water to produce C-S-H gel. Fly ash is considered as a solid waste, but it can be beneficially used to make PCPC, preventing FA from taking unnecessary space in landfills (Pando and Hwang, 2006). By substituting part of the Portland cement with FA one can reduce carbon dioxide production during the production of cement and financial burdens of solid waste management. Portland cement pervious concrete can be used to control runoff in terms of quantity and quality. Past research has shown that PCPC is capable of separating solid material from runoff and pollutants (Luck et al., 2008; Park and Tia, 2004).

The goal of this research was to obtain the optimum mixture design of PCPC for runoff controls in terms of volume reduction and quality enhancement. Different materials were used to develop PCPC with the highest possible compressive strength, while retaining a good permeability. An industrial byproduct, FA and engineered iron oxide nanoparticles coated with surfactants ($ENP_{Fe\text{-}surf}$) were used as the main additives to PCPC for the purpose of solid waste valorization and material innovation, respectively, in addition to enhance the PCPC properties. To meet this end, a series of lab-scale investigations were conducted to:

1) evaluate possible contribution of FA and $ENP_{Fe\text{-}surf}$ to strength and durability of cement paste and PCPC;
2) obtain the optimum ratios of water-binder , Fly ash-binder and $ENP_{Fe\text{-}surf}$ powder for PCPC using a two level central composite factorial design;
3) test phosphorus removal with the optimized PCPC; and
4) assess effective PCPC regeneration by Fenton oxidation with embedded $ENP_{Fe\text{-}surf}$.

2. LITERATURE REVIEW

2.1 Stormwater Runoff

With human population and activities being increased, urbanization of available land can increase and this increases impervious surfaces. The Environmental Protection Agency (EPA) defines the stormwater runoff as water generated by precipitation or melting snow, which does not percolate through impervious surfaces and carries with it debris, chemical compounds, sediments and other pollutants to surface waters or pervious soil where it can recharge groundwater. The pollutants carried by runoff can potentially adversely affect water quality when left untreated. Urban and suburban areas' pollutants include: sediments, oil and other chemical compounds from motor vehicles, pesticides, nutrients, microorganisms from animal wastes or failing septic systems and others (EPA, 1999).

Depending on the land use, the presence of certain pollutants can be observed. Nutrients (nitrogen and phosphorus), heavy metals, oil grease and particle matter have been found in highway runoffs (Kim et al., 2005). The presence of these pollutants was associated with the automobile traffic and the land use alongside highways. One example of land uses is land development intended for agricultural purposes. Yang et al. (2013) compared different land uses. One of their findings was that the highest phosphorus concentration in runoffs occurred on vegetable farms. Another thing was that pollutant loads, such as total phosphorus, total nitrogen and metals, depended on rainfall events. In other words, as the rain event increased so did the loads.

The type of surface also affects the presence of pollutants in runoff. A study compared the quantity and quality of runoff production on asphalt, permeable paver and crushed-stone driveways. The researchers found that the permeable paver and crushed-stone decreased runoff volume and concentrations of total suspended solids (TSS) and nutrients (nitrogen and phosphorus) (Gilbert and Clausen, 2006). This highlights the importance of reducing impervious surfaces, such as asphalt and concrete, in order to reduce runoff and pollutants associated with runoff.

Phosphorus, like nitrogen, is a nutrient that is necessary for plant growth. A problem arises when both nutrients are present in great quantities, resulting in eutrophication in surface waters (Chapra, 1997). The importance of monitoring phosphorus is that even if it is present in short periods of time, a moderate increase of its presence can provoke algae bloom, decrease dissolve oxygen and consequently induce the death of aquatic animals (EPA, 1999). Elemental phosphorus is rare in nature; usually it is present as phosphate. The EPA has established as maximum permitted total phosphorus concentration for surface water to be 1 mg/L (EPA, 2010).

2.2 Portland Cement Pervious Concrete

A possible solution for runoff and related pollutant transport is the use of PCPC. Portland cement pervious concrete, permeable concrete or no-fine concrete is a material used in construction, which is always made of Portland cement, coarse aggregate, air and water, but it can include other materials. The allure of PCPC comes from its permeability, which prevents water ponding after rain and can reduce or even eliminate runoff. Some of its advantages over common impervious concrete are: capacity to control runoff related pollution, decrease or elimination of water-detention ponds, elimination of water ponding in the surface, reduction of road surface glare, mitigation of heat island effect, and filtration of water that can reach tree roots

and groundwater. It has been used in parking lots, parks, tennis court, swimming pool deck, and floors for zoo areas or animal barns (ACI, 2010; Garber, 2010). Other uses include sewage treatment plant sludge beds, solar energy storage systems and artificial reefs (ACI, 2010). Its usage has been documented since mid-1900s by the American Concrete Institute (Garber, 2010). Although it has many advantages, its low compression and flexural strengths limits its traffic load capacity, it cannot be used on the top of expansive soil and it has long curing time. Also when it is used in construction sites, it may need stabilizers that can slow down its hardening time (Garber, 2010).

As mentioned previously, PCPC is mainly composed of coarse aggregate, Portland cement, air and water, but is not limited by these materials. Portland cement pervious concrete mixtures can also have fine aggregate, fibers, and mineral or chemical admixture. Its initial absence of fine aggregate such as sand is what gave one of its names no-fine concrete, although nowadays small amounts are used in some cases (Huang et al., 2010). Mineral admixtures with pozzolanic activity are the powders that can react with calcium hydroxide, in presence of water, at ordinary temperature to form compounds possessing cementitious properties (ASTM C618). By adding mineral admixtures, such as FA and silica fume, one can reduce the amount of Portland cement needed. Chemical admixtures are chemical compounds added to the mixture to enhance the properties of the PCPC such as workability and strength (Garber, 2010).

In order to make PCPC that has continuous void, one has to make a paste that has the right consistency. The consistency of the paste is greatly affected by the water-to-cement ratio. If the water-to-cement ratio is too low, the paste will have bad workability and some of the cement could stay dry and the paste won't cover the aggregate properly on the other hand, if the water-to-cement ratio is too high, the paste will drip off the aggregate towards the bottom resulting in

sealing the bottom (Garber, 2010). Garber (2010) recommended the range of water-to-cement ratio to be 0.27 to 0.34 (by mass). Getting the correct proportions of the materials used to prepare PCPC is of great importance. Sonebi and Bassouni (2013) used a statistical modeling in order to obtain the aggregate amount, cement amount and water-to-cement ratio needed to make good PCPC specimen.

Past research has found that as the void ratio increased, the permeability increases and the compressive and tensile strengths decreased. In order to make a PCPC that can withstand traffic load its compressive and flexural strength have to be increased. Decreasing void ratio and consequently its permeability usually do this. Different approaches have been used by past research in order to increase compressive strength. It has been found that decreasing the aggregate size could increase compressive strength, but it decreased permeability (Yang and Jiang, 2003). Chen et al. (2013) compared mixtures modified with pozzolans and with a polymer. They found that the PCPC modified with mineral admixture (Class C FA and silica fume) had a more rapid increase in compressive strength at early curing stages (7 days) when compared to the PCPC modified with the polymer. The specimens modified with mineral admixtures could still increase its compressive strength if more curing time was given, although the specimens modified with the polymer reached higher compressive strength after 90 days of curing (Chen et al., 2013).

2.3 Portland Cement

One of the principal components of the PCPC is Portland cement. Portland cement comes from granulated clinkers and is composed of tricalcium silicate (C_3S or $3CaO•SiO_2$), dicalcium silicate (C_2S or $2CaO•SiO_2$) tricalcium aluminate (C_3A or $3CaO•Al_2O_3$), and tretracalcium aluminoferrite (C_4AF or $4CaO•Al_2O_3•Fe_2O_3$) (ATSM C 150). The hydrated cementitious paste

is mainly composed of 50 to 65% calcium silicate hydrate (known as C-S-H gel), from 20 to 25% of calcium hydroxide (known as Portlandite), from 15 to 20% of hydrated calcium sulfoaluminatehydrates and unhydrated clinker (Mehta and Monteiro, 2013).

Tricalcium silicate reacts with water faster than dicalcium silicate, which makes it responsible for early age strength. Both specimens react with water to produce calcium silicate hydrate (C-S-H gel or $CaSiO_2 \bullet 2H_2O$). On the other hand dicalcium silicate produces less amount of calcium hydroxide than tricalcium silicate, which is highly soluble and does not contribute to the concrete strength. Tricalcium aluminate and tetracalcium aluminoferrite do not contribute to concrete strength, but are included for economic reasons. In the absence of sulfate ions (SO_4^{2-}) tricalcium aluminate along with water can produce calcium aluminate hydrates. This reaction is very rapid and is undesirable; consequently gypsum or calcium sulfate dihydrate ($CaSO_4 \bullet 2H2O$) is added to Portland cement in order to delay its setting time (Mehta and Monteiro, 2013). Tricalcium aluminate reacts with calcium sulfate dihydrate producing ettringite ($((CaO)_6(Al_2O_3)(SO_3)_3 \bullet 32H_2O$), which is a slower reaction. The problem arises when there is not enough calcium sulfate dihydrate to react with all of the tricalcium aluminate present; ettringite becomes unstable and converts to monosulfoaluminate. If more ions of sulfate enter the mature cementitious matrix monosulfoaluminate will convert to ettringite, which occupies a larger volume causing internal pressure that leads to cracks. Tetracalcium aluminoferrite goes through reactions similar to tricalcium aluminate, but iron is present instead of aluminum (Mehta and Monteiro, 2013).

2.4 Fly Ash

In the United States, 42% of the electricity was produced via coal combustion in 2011 (EIA, 2013). The use of coal for electricity generation produces different combustion by-

products including FA, which will be considered as a solid waste unless a validation, is accomplished for it. More than 280 Mt of FA and bottom ash combined is produced annually (Kovler, 2012). Fly ash has been used in asphalt and concrete pavement, for soil stabilization, as a soil buffer, as an adsorbent of chemical compounds, in the synthesis of zeolite and other applications (Ahmaruzzaman, 2010; Pandey and Singh, 2010; Wang and Wu, 2006). It has also been studied for the removal of phosphate in aqueous solutions (Agyei et al., 2002). Fly ash is a fine powder with a particle size ranging from 10 to 100 μm and it is produced during the coal combustion process (Pando and Hwang, 2006). Its chemical composition depends on the chemical composition of the coal used in the combustion.

The motivation for this work was to substitute part of the Portland cement needed to prepare PCPC with FA can reduce the costs, carbon dioxide production due to the fabrication of Portland cement, and burdens of solid waste management. FA can also increase compressive strength with time due to pozzolanic activity (Chindaprasirt et al., 2004). Chindaprasirt et al. (2004) found that FA was capable of reducing drying shrinkage, reducing the expansion related to sulfate attack and increasing resistance to sulfuric acid attack of cement mortars. Chang et al. (2005) measured compressive strength of concrete cylinders after 168 days of being immersed in 1% sulfuric acid. The concrete cylinders that had limestone aggregate, FA, and silica fume had the smallest change in compressive strength. The addition of FA to PCPC can potentially increase its compressive strength by increasing its paste strength. It can also protect PCPC from acid attack and help in the removal of phosphorus. The SiO_2 present in FA reacts with calcium hydroxide to form more C-S-H with a composition with a reduced Ca/Si ratio. This reaction, known as pozzolanic reaction, is a slow reaction that generally does not initiate before 7 days (Deschner et. al, 2012).

2.5 Iron Oxide Nanoparticles

Nanoparticles are the materials that range from 1 and 100 nm in all three dimensions. Nanoparticles have been used in a variety of fields including: environmental remediation, cosmetics, pharmaceutics, medicine, electronics and catalysis (Ju-Nam and Lead, 2008). Nanoparticles have been suggested as an alternative in environmental remediation due to their efficiency, cost-effectiveness and eco-friendly characteristics (Xu et al., 2012). Nanoparticles have the capacity of improving early-age mechanical properties of cementitious materials including those with FA added (Kawashima et al., 2013). Nanoparticles are usually grouped as carbon-based, quantum dots and metal oxides.

Metal oxides have been used in the food industry, environmental remediation, biological sciences, cosmetics, sunscreen products, catalysis and dental medicine (Ju-Nam and Lead, 2008). Nanoparticles such as SiO_2, Al_2O_3 and Fe_2O_3 have being added to cement mortar in order to increase its compressive strength (Li et al., 2004; Oltulu and Sahin, 2013). The increase of compressive strength in cement mortar with SiO_2 or Fe_2O_3 added can be seen at the standard 7 and 28 day curing when compared to cement mortar without nanoparticles (Sanchez and Sobolev, 2010).

Metal oxides include iron oxide, which exists in a variety of forms including magnetite (Fe_3O_4), maghemite (γ-Fe_2O_3), and hermatite (α-Fe_2O_3) (Xu et al., 2012). Hematite has oxygen atoms closely packed around Fe^{3+} ions, has a high stability and relative low cost. Maghemite has the same composition that hematite, same physical structure of magnetite and can be considered as fully oxidized (Fe^{2+}). Magnetite has a structure where oxygen ions form a face-centered cubic lattice and the Fe ions occupy tetrahedral and octahedral sites and is one of the most highly magnetic of the iron oxides (Park et al., 2008). Iron oxide nanoparticles have been used in

medical applications, such as cancer diagnosis, manufacture of pigments and water treatment plants (Ju-Nam and Lead, 2008; Xu et al., 2012). Iron based magnetic like magnetite have being studied for treatment of polluted water, used for surface adsorption target compounds such as heavy metals and phosphate (Daou et al., 2007; Tang and Lo, 2013). The iron oxide nanoparticle used in this research was magnetite covered by a proprietary surfactant to prevent its agglomeration in the aqueous solution.

2.5 Durability of the Cementitious Paste in PCPC

Concrete can be damaged by physical and chemical processes. Physical processes include erosion, abrasion, cavitation, crystallization of salts in pores, structural loading, freeze/thaw damage, and temperature and moisture changes. Chemical deterioration includes hydrolysis of cement paste components, sulphate attack, acid attack, carbonation, and seawater exposure (ACI, 2000; Mehta and Monteiro, 2013). Hydrolysis of cement components occurs due to the high solubility of calcium hydroxide. When the cement paste is in contact with water that has low concentration of calcium such as soft water, rainwater, and deionized water; calcium hydroxide will diffuse out of the cement paste (Mehta and Monteiro, 2013). Sulfate attack is responsible for the formation of expansive reaction product such as gypsum, ettringite, brucite, and thaumacite (ACI, 2000; Hossain and Lachemi, 2006). The effects of sulfuric attack are usually related to weight changes in concrete specimens. These expansive reaction products cause internal pressure that lead to cracks and spalling. When a cementitious paste is in contact with an acid, the H^+ ions in the acid it promotes the dissolution of calcium hydroxide and calcium carbonate (Makhoufi et al., 2012). Concrete can come into contact with organic acid such as acetic, propionic, lactic, in agriculture, food industry and trough natural environment, such as decomposition (Bertron et al., 2005a; Mehta and Montero, 2013). Organic acids usually degrade

more cementitious paste than strong acid when compared with a given pH value due to the organic acid's higher concentration (Gruyaert et al., 2012). Sulfuric acid in particular can be particularly detrimental due to the simultaneous acid and sulfate attack (Makhoufi et al., 2012). Magnesium which is present in hard water can enter cementitious matrix and produce magnesium hydroxide (brucite or $Mg(OH)_2$), which is an expansive compound. With time the magnesium ions can even substitute calcium ions in the calcium silicate hydrate, as consequence the concrete will lose cementitious properties (Mehta and Monteiro, 2013). Marine water has the presence of many ions such as sodium (Na^+), chloride (Cl^-), sulfate (SO_4^{2-}), and magnesium (Mg^{2+}). Marine environments such as those found in Puerto Rico are a complex case since different processes and mechanisms of attack can occur simultaneously (ACI, 2000; Mehta and Monteiro, 2013).

2.6 Response Surface Methodology

Experimental design contributes to scientific and engineering development by decreasing experimental time and cost. This reduction can be accomplished by reducing the total amount of experimental runs while assuring that all possible variable combinations will be taken into consideration. Response surface methodology is an example of experimental design. Response Surface Methodology (RSM) can assess the statistical relevance of more than one variable and its interaction for one or more desired responses (Montgomery, 2009). RSM has been used in biology, chemistry and engineering to optimize products or processes (Nambiar and Ramamurthy, 2006). In order to find the best mixture design that includes water-to-binder ratio, partial substitution of Portland cement by FA and iron oxide nanoparticles addition a RSM was utilized. A second order model is used in order to describe the effect a group of factors have on one or more responses. The second order polynomial used in RSM is of the form shown in

equation 1. The β_0 is the intercept coefficient, β_i, β_j and β_k are the linear coefficients, β_{ii}, β_{jj}, and β_{kk} are the quadratic coefficients and β_{ij}, β_{ik}, and β_{jk} are the coefficients of the interactions (Mehta et al., 2014; Mohammed et al., 2012). Central composite design (CCD), like the one shown in Figure 1, is a popular model that fits the second order model (Montgomery, 2009). The CCD used in the current study consisted of a 2^3 factorial (8 runs), 6 axial runs and 6 center runs.

$$y = \beta_0 + \beta_i x_i + \beta_j x_j + \beta_k x_k + \beta_i {x_i}^2 + \beta_j {x_j}^2 + \beta_k {x_k}^2 + \beta_{ij} x_i x_j + \beta_{ik} x_i x_k + \beta_{jk} x_j x_k \qquad (1)$$

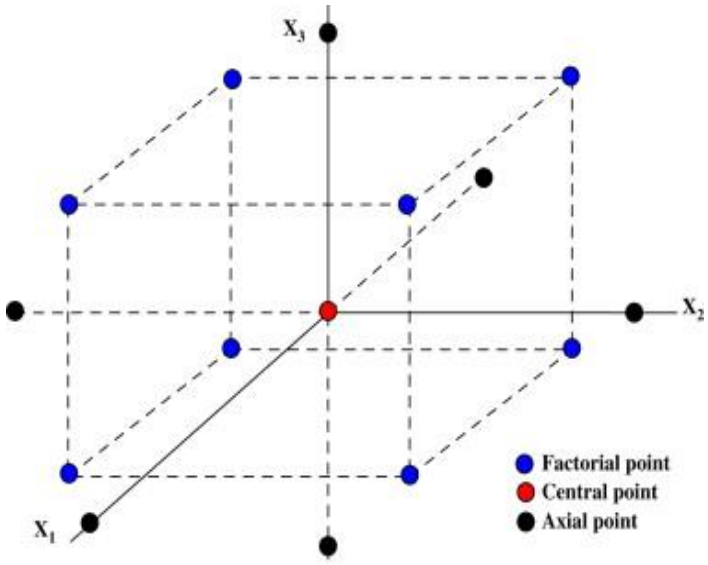

Figure 1. A 2^3 central composite design

(source: Cho and Zoh, 2007)

2.7 Clogging of Portland Cement Pervious Concrete and Fenton Regeneration

As with any filters, PCPC is susceptible to clogging and therefore reduction of permeability. Portland cement pervious concrete can get clogged with inorganic and organic

matters as time passes by. It has been found that finer particulate matters can gradually clog PCPC as the loading increases, decreasing the hydraulic conductivity. Periodical maintenance like sonicating/vacuuming and vacuuming can restore over 96% of the original hydraulic conductivity (Sansalone et al., 2012). Chopra et al. (2010) compared vacuum sweeping and pressure washing and found pressure washing to be more effective. They also found that the majority of the clogging materials were silty fine sand. Kayhanian et al. (2012) statistically compared the permeability of 20 parking lots and found that the age of the PCPC and the mass of fine particles less than 38 μm are the variables that are affected the most, although most of the sediment found were related to particles larger that 38 μm.

Bio-clogging occurs when bacteriological activity produces material that fills soil pores reducing its hydraulic conductivity. This can be accomplished by the production of microbial slime including exopolysaccharides (Ivanov and Chu, 2008). Microaerophilic bacteria such as *Beggiatoa*, *Haliscomenobacter*, *Microthrix*, *Nocardia*, *Spaerotilus* and *Thiothrix* are common in aerobic tanks of wastewater treatment plants that can be used to enhance bioclogging. Also facultative aerobic and anaerobic bacteria are suitable to enhance bio-clogging of the PCPC due to their large production of exopolysaccharides.

Advance oxidation process has been used to treat industrial and domestic wastewater in order to remove inorganic and organic pollutants. An example of advance oxidation process is Fenton oxidation. This oxidation takes place when hydrogen peroxide and iron react to produce hydroxide radicals as shown in equations 2and 3.

$$H_2O_2 + Fe^{2+} \rightarrow Fe^{3+} + HO^- + HO^{\cdot} (k = 63.0 L/mol \cdot s) \quad (2)$$

$$H_2O_2 + Fe^{3+} \longrightarrow Fe^{2+} + HO_2^{\cdot} + H^+ \ (k = 3.1 \times 10^{-3}\ L/mol \cdot s) \quad (3)$$

Both hydrogen peroxide and hydroxyl radical are strong oxidants and hydroxyl radicals is an extremely powerful oxidant, second only to fluorine (Neyens and Baeyens, 2003). A combination of coagulation and Fenton oxidation has been used in order to decrease TSS, chemical oxygen demand, biological oxygen demand, phosphate, heavy metals, dyes and other chemical substances (Badawy and Ali, 2006). Electro-Fenton oxidation was used to remove a high percentage of coliform from landfill leachate (Aziz et al., 2013). Fenton reaction can be carried out homogeneously or heterogeneously. Rusevova et al. (2012) performed a heterogeneous Fenton reaction using magnetite nanoparticles in order to remove phenol. It should be mentioned that it was found that part of the magnetite is converted to maghemite in the presence of hydrogen peroxide, thus decreasing its efficiency. In order for the Fenton oxidation to effectively occur the medium should be in acidic conditions, although when it is carried out heterogeneously it can take place at higher pH values (Nieto-Juarez, 2012). Different experiments have shown that acid can decrease the mass and compressive strength of cement concrete (Fan et al., 2010; Xie et al., 2004). Although cement concrete is susceptible to acid attack, FA could decrease such damaging effect. Fly ash could protect the PCPC from a reduction in pH when a Fenton oxidation is carried out in an acidic environment (Chindaprasirt et al., 2004; Temuujin et al., 2011).

3. MATERIALS

The PCPC mixture included Portland cement, potable water and coarse limestone gravel in sizes with passing through 9.5 mm sieve, but retaining on 4.75 mm sieve. The water temperature used for the mixture and for curing the specimens was not controlled. All materials were obtained from local suppliers.

The Portland cement is from CEMEX Type IP and complies with ASTM C595. The specific gravity of the Portland cement is 2.86. Scanning electron microscopy (SEM) image of Portland cement used in this research is shown in Figure 2. The chemical composition was obtained from XRF (Essroc San Juan) and are shown in Table 1.

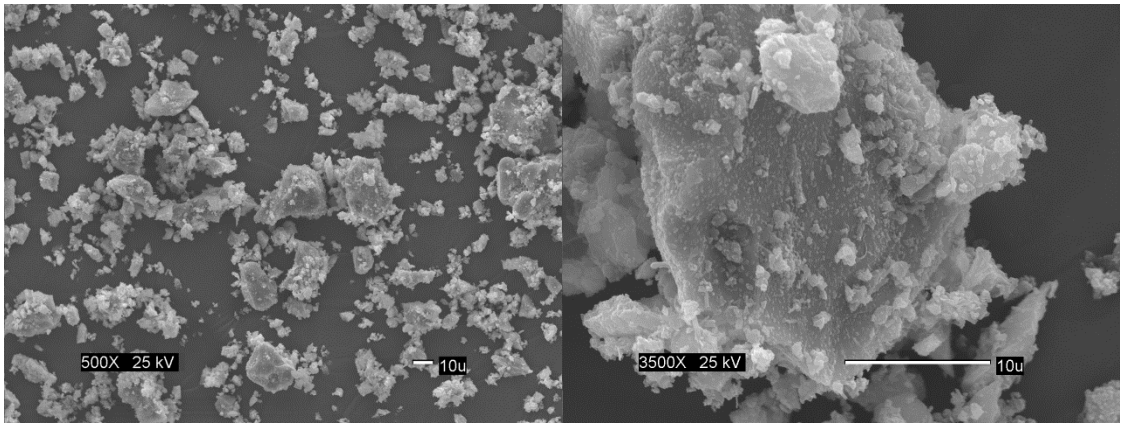

Figure 2. Scanning electron microscopy image of Portland cement Type IP

Table 1 Chemical composition of Cemex Portland cement

Chemical composition of Portland cement				
SiO_2	Al_2O_3	Fe_2O_3	CaO	MgO
27.14	6.68	3.71	55.47	1.62
SO_3	Na_2O	K_2O	TiO_2	P_2O_5
3.48	0.59	0.48	0.32	0.11

FA was donated by the AES Puerto Rico. The FA has a specific gravity of 2.55 and the SEM image obtained is shown in Figure 3. The chemical composition of the FA was obtained from XRF (Essroc San Juan) and is presented in Table 2. The FA utilized in this research does not comply with ASTM C 618, as its SO_4 content is higher than 5%. Regardless of this, it is desired to study the possible incorporation of this particular FA in order to diversify it usage in Puerto Rico and decrease the amount of FA that is being sent to landfills. Furthermore, a long-term curing is not the norm in the field, therefore a seven-day curing time was preferred in order to design a material with properties closer to those obtained in the field regardless of the slow kinetic of the pozzolanic reaction.

Table 2. Chemical composition of AES PR fly ash

Chemical composition of fly ash				
SiO_2	Al_2O_3	Fe_2O_3	CaO	MgO
30.84	9.93	5.01	39.61	0.35
SO_3	Na_2O	K_2O	TiO_2	P_2O_5
11.43	0.90	1.01	0.45	0.11

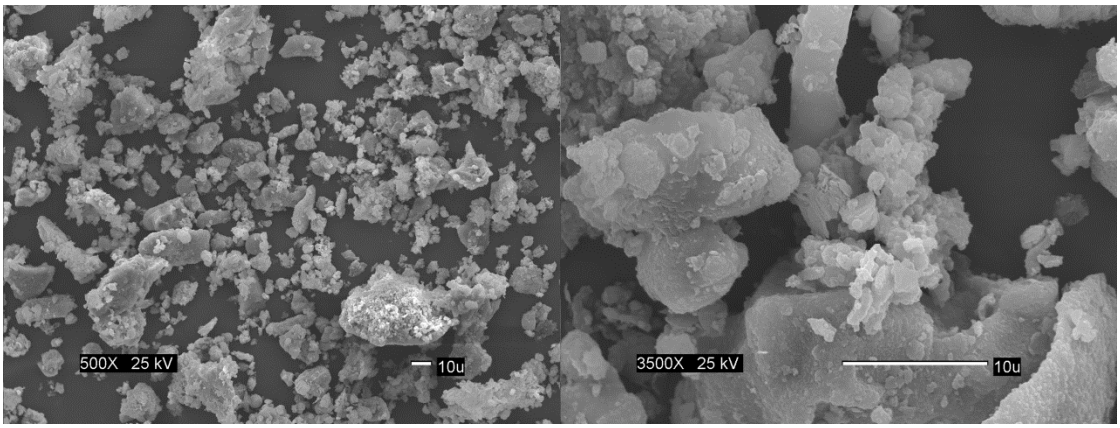

Figure 3. Scanning electron microscopy image of AES fly ash

Iron oxide nanoparticles coated with surfactant ($ENP_{Fe\text{-}surf}$) were obtained from Ferrotec (MSG W10). The surfactant is a proprietary material from Ferrotec, therefore its chemical composition is not disclosed. The chemical and physical characteristics of the $ENP_{Fe\text{-}surf}$ are shown in Table 3.

Table 3. Characteristics of engineered iron oxide nanoparticles coated with surfactant

Parameter		Value or Description
Composition (% by vol.)	Magnetite	2.8 - 3.5
	Surfactant	2.0 - 4.0
	Water	92.5 - 95.2
Appearance		black fluid
Nominal particle diameter		10 nm
Density		1.245 g/mL
pH		> 10

4. Methodology

4.1 Cementitious Pastes

Four combinations of cementitious paste mixture were compared and each material combination is shown in Table 4. All four combinations had a ratio of water-to-binder ratio at 0.35. The consistency of the fresh pastes was compared using a flow table (in accordance with ASTM C230) following ASTM C 1437. The consistency or percentage of spread was calculated using equation

4 and the process is shown in Figure 4. Setting time was measured with a Vicat Needle as established in ASTM C 191. The Vicat needle is shown in Figure 5.

Table 4. Combinations of cementitious pastes

Cementitious Pastes		
Mixture ID	FA/B (%)	ENP/B (%)
P-1	0	0
P-2	40	0
P-3	0	3
P-4	40	3

$$\%\ of\ spread = \frac{(D_f - D_i)}{D_i} \quad (4)$$

Figure 4. Description of fluidity measurement with the flow table

Figure 5. Vicat needle used to measure setting time

(source: UKY, 2014)

A short-term chemical attack was assessed for all 4 cementitious pastes. The specimens were demolded after 24 hours and were placed in each corresponding solution. The solutions were deionized water, sulfuric acid (0.01% v/v and pH 3) and NaCl (5% w/v). The specimens

were in each solution for 11days. After the 11 days all specimens were air dried for 24 hours and were tested for compressive strength.

A long-term acid attack was also tested on all four combinations. The specimens were demolded 24 hour after preparation, were cured in potable water (with lime) for 28 days. Two specimens prepared with each combination were placed in contact with either sulfuric or acetic acid. Each acid solution was intended to have a pH value of 3. After 3, 7, 28, 56 and 90 days each specimen surface was rinsed, blob dried and weighted. The change in mass was compared to the mass after 1 day in each solution by using equations 5 and 6. After 90 days the specimens were tested for compressive strength.

$$M_{gained}(\%) = \frac{M(t)}{M(t_0)} - 1 \quad (5)$$

$$M_{lost}(\%) = 1 - \frac{M(t)}{M(t_0)} \quad (6)$$

4.2 Portland Cement Pervious Concrete Mixtures Design

The statistical model RSM was used in order to design the PCPC mixture. The model had 3 factors with two levels (full factorial) each. The central composite design was chosen. Two replicates were made. Three variables (factors) that were tested are: water-binder ratio (W/B), Fly ash-binder ratio (FA/B), and $ENP_{Fe\text{-}surf}$-binder ratio (ENP/B). The amount of binder (Portland cement and FA) depended on the amount of coarse gravels used, which depended on the amount of specimens obtained from each mixture. The coarse gravel to cement ratio was 4:1 for all mixture designs. The proportions of each material are mass based. Each of the mixtures was designed to obtain three specimens; two to test compressive strength and the other to test

permeability, void content and hardened density. The water added to each mixture depended on the moisture content of the gravel utilized and on the amount of water present in the ENP solution added. The two levels of W/B were 34 and 40% and the axial points were 32.1 and 41.9%. For FA/B, the levels were 10 and 40% with the axial points of 0.5 and 49.5%. The levels of ENP/B were 1 and 5% and its corresponding axial points were 0.3 and 6.3%. Table 5 shows a summary of the factors and each level for the model. The amount of gravel, cement, FA, ENP solution and water utilized are presented in

Table 6. The model was used to obtain the optimum mixture with acceptable compressive strength, permeability, void content, and density values. The specimens prepared with the optimum design were tested for its compressive strength, permeability, void content and density to test the accuracy of the RSM results. This optimum mixture was used to test its capacity of phosphorus removal.

Table 5. Factors and each factor levels for the RSM

Factor	Low level	High level
W/B	34	40
FA/B	10	40
ENP/B	1	5

Table 6. Amount of gravel, cement, FA, ENP and water added to each mixture

Block	W/B Ratio (%)	FA/B Ratio (%)	ENP/B Ratio (%)	Gravel (g)	Cement (g)	Fly Ash (g)	ENP (g)	Water[a] (g)
1	34.0	10.0	1.0	7538.6	1696.2	188.5	18.8	666.7
1	40.0	40.0	1.0	7538.6	1130.8	753.9	18.8	754.6
1	40.0	10.0	5.0	7538.6	1696.2	188.5	94.2	722.9
1	34.0	40.0	5.0	7538.6	1130.8	753.9	94.2	584.6
1	37.0	25.0	3.0	7538.6	1413.5	471.2	56.5	694.8
1	37.0	25.0	3.0	7538.6	1413.5	471.2	56.5	669.6
2	40.0	10.0	1.0	7538.6	1696.2	188.5	18.8	790.0
2	34.0	40.0	1.0	7538.6	1130.8	753.9	18.8	676.9
2	34.0	10.0	5.0	7538.6	1696.2	188.5	94.2	615.2
2	40.0	40.0	5.0	7538.6	1130.8	753.9	94.2	733.1
2	37.0	25.0	3.0	7538.6	1413.5	471.2	56.5	705.0
2	37.0	25.0	3.0	7538.6	1413.5	471.2	56.5	705.0
3	32.1	25.0	3.0	7538.6	1413.5	471.2	56.5	522.6
3	41.9	25.0	3.0	7538.6	1413.5	471.2	56.5	717.4
3	37.0	0.5	3.0	7538.6	1875.1	9.5	56.5	635.5
3	37.0	49.5	3.0	7538.6	951.8	932.8	56.5	635.5
3	37.0	25.0	0.3	7538.6	1413.5	471.2	5.0	651.7
3	37.0	25.0	6.3	7538.6	1413.5	471.2	118.1	565.2
3	37.0	25.0	3.0	7538.6	1413.5	471.2	56.5	597.5
3	37.0	25.0	3.0	7538.6	1413.5	471.2	56.5	614.1
4	34.0	10.0	1.0	7538.6	1696.2	188.5	18.8	656.7
4	40.0	40.0	1.0	7538.6	1130.8	753.9	18.8	769.8
4	40.0	10.0	5.0	7538.6	1696.2	188.5	94.2	723.4
4	34.0	40.0	5.0	7538.6	1130.8	753.9	94.2	610.3
4	37.0	25.0	3.0	7538.6	1413.5	471.2	56.5	695.3
4	37.0	25.0	3.0	7538.6	1413.5	471.2	56.5	684.8
5	40.0	10.0	1.0	7538.6	1696.2	188.5	18.8	788.8
5	34.0	40.0	1.0	7538.6	1130.8	753.9	18.8	671.1
5	34.0	10.0	5.0	7538.6	1696.2	188.5	94.2	610.0
5	40.0	40.0	5.0	7538.6	1130.8	753.9	94.2	723.1
5	37.0	25.0	3.0	7538.6	1413.5	471.2	56.5	695.0
5	37.0	25.0	3.0	7538.6	1413.5	471.2	56.5	699.3
6	32.1	25.0	3.0	7538.6	1413.5	471.2	56.5	550.8
6	41.9	25.0	3.0	7538.6	1413.5	471.2	56.5	735.5
6	37.0	0.5	3.0	7538.6	1875.1	9.5	56.5	669.1
6	37.0	49.5	3.0	7538.6	951.8	932.8	56.5	684.2
6	37.0	25.0	0.3	7538.6	1413.5	471.2	5.0	708.0
6	37.0	25.0	6.3	7538.6	1413.5	471.2	118.1	637.7
6	37.0	25.0	3.0	7538.6	1413.5	471.2	56.5	643.1
6	37.0	25.0	3.0	7538.6	1413.5	471.2	56.5	669.1

[a]Water quantity was adjusted depending on gravel moisture content and the water content of $ENP_{Fe\text{-}surf}$ solution used.

4.2.1 Portland Cement Pervious Concrete Specimen Preparation

The mixtures were prepared in a mechanical mixer. The coarse aggregate and binder were placed in the mechanical mixer and mixed for 1 minute. The water (with the $ENP_{Fe\text{-}surf}$) were

later added and mixed for 3 minutes. The mixtures were transferred to cylindrical molds 20 cm long and 10 cm of diameter (8 in and 4 in). After each addition of mixtures into the mold, the mixtures were compacted with a rod in accordance to ASTM C 192. The specimens were cured in potable water (with calcium hydroxide). Compression and permeability tests were done for 7-day cured specimens to obtain optimum PCPC design by the RSM. After acquiring optimum PCPC mixture design, compressive strength tests were made with the specimens cured for 3, 7, 28, 56 and 90 days.

4.2.2 Measurement of Responses of Portland Cement Pervious Concrete for RSM

The compressive strength test was done in accordance with ASTM C39. Compressive axial load was applied to each specimen until failure occurred. Rubber caps were used to evenly distribute the load on the top and bottom parts of the specimens. Figure 6 shows a PCPC specimen being tested.

Figure 6. PCPC being tested for compressive strength

The permeability was assessed by a constant head method that was modified from ASTM D 2434. The equipment is shown in Figure 7. A constant water column was maintained while water flows through the specimen. Time was measured as the effluent fills a specific volume in

order to obtain the flow rate. Using the surface area and the length of the specimen, the permeability was calculated using **Error! Reference source not found.**; where V_w is the water olume, L is the length of the PCPC specimen, D is the diameter, Δh is the constant water head, and t is the time. The permeability is reported in mm/s.

$$Permeability = \frac{V_w L}{\frac{\pi}{4} D^2 \Delta h t} \quad (7)$$

Figure 7 Permeability test setup

The measurement of void content and density of hardened pervious concrete complies with ASTM C1754. Equations 8 and 9 were used, where the void content is in percentage and the density is in kg/m^3. The M_{od} is the oven dried specimen (35 °C) and the M_{sw} is the submerged specimen.

$$Void\ Content = \left(1 - \left(\frac{M_{od} - M_{sw}}{\rho_w D^2 L}\right)\right) \times 100\% \quad (8)$$

$$Density = \frac{M_{od}}{V} \quad (9)$$

4.2.3 Water Quality Tests

Taking into consideration the $ENP_{Fe\text{-}surf}$ utilized in this research is costly, the specimens prepared following the optimum design were tested for possible iron leaching. It is imperative that the $ENP_{surf\text{-}Fe}$ used stay within the cementitious matrix. The method used to measure the total iron cannot differentiate iron leached from the nanoparticles, Portland cement, or the FA. Therefore a comparison between the optimum and control design was accomplished. The design is shown in Table 7. After 24 hours the specimen were demolded and placed in water for 12 days. In each container two specimens were placed (5 cm of diameter and 10 cm of length) with an effort to minimize variability among the specimens during compaction. Water was replenished after each water sample was taken. The iron concentration was measured using HACH Method 8008. The experiment was stopped after 12 days because no iron concentration was detected (lower detection limit: 0.02 mg/L). It was done in duplicates for each PCPC design.

Table 7. Designs of controls

Design of Controls			
ID	W/B	FA/B	ENP/B
C-1	34	0	0
C-2	34	15	0
C-3	34	0	5

The specimens made with optimized PCPC design were tested for its capacity for phosphate reduction. For this purpose, two tests were conducted. In both test phosphate concentration was measured with HACH Method 8190 as shown in Table 9. The first test was a kinetic experiment where two specimens were placed in a container. Phosphate concentrations along with pH were measured at time intervals. On the second test twelve specimens, with 5 cm of diameter and 10 cm of length each, were placed on six containers (two specimens in each container). The containers had different concentrations, which are shown in Table 8. All specimens utilized in both experiments were cured for 7 days. After 72 hours, pH and phosphate concentration were measured. In both studies each container had 2 L of $Na_2HPO_4 \bullet 7H_2O$ solution at the intended initial phosphate concentration. Both studies were also conducted for controls, which are shown in Table 7. All specimen utilized in both experiments were cured for 7 days. The 1st order phosphate removal constant and both Freundlich's coefficients (K_f and 1/n) were obtained.

Table 8. Concentrations of phosphate solution for Adsorption Isotherm

Concentration of phosphate solution						
Container's ID	1	2	3	4	5	6
Concentration (mg/L)	1	2.5	5	10	25	50

Table 9. Water quality parameters to be tested

Parameter	Instrument	Method
pH	Milwaukee pH600 meter	Insert pH meter into the water sample
Total Iron	HACH DR 2800	HACH Method 8008 FerroVer Iron Reagent Powder Pillow
Total Phosphorus	HACH DR 2800	HACH Method 8190 Total Phosphorus Test 'N Tube Reagent Set

4.2.4 Fenton Regeneration

Dilute hydrogen peroxide solution at a concentration of 0.1% was used to unclogg cylindrical specimens of PCPC. The produced hydroxyl radicals are expected to regenerate the clogged PCPC by oxidizing both biogenic and abiogenic materials within the PCPC pores. Regeneration effectiveness was assessed in terms of permeability. Compressive strength was analyzed after Fenton regeneration to asses potential impact of oxidation on structural property.

The specimens (20 cm of length and 10 cm of diameter) were placed in 100-L container. One container had all 10 specimens that were made with the optimum design. The other container had the specimen made with control-2 design (Table 7). Each container was filled with 50 L of water from a nearby creek, which was replenished for the first 4 days. In order to accelerate clogging process, on the fifth day the water was spiked with bacteria that are used for seeding in BOD test (Polyseed, Interlab). Glucose (10 g) and the nutrients listed in Table 10 were also added to the water daily. However, no visual clogging was observed even after 4 additional days. Therefore the creek water was loaded with 50 mL of activated sludge collected from the Mayaguez Wastewater Treatment plant. Figure 8 shows the reservoir containing the specimens C-2 after the water was loaded with activated sludge.

Table 10. Nutrient concentration fed daily to the microorganism

Nutrient	Concentration (g/L)
$CaCl_2$	36.43
$FeCl_3$	0.3199
$MgSO_4 \cdot 7H_2O$	22.5
NH_4Cl_2	1.7
KH_2PO_4	8.5
$Na_2HPO_4 \cdot 7H_2O$	33.4

Figure 8. Specimens (design C-2) in water reservoir loaded with activated sludge

Once the PCPC specimens appeared to be covered with “slime”, two random specimens were taken to measure permeability. All 20 specimens were placed in hydrogen peroxide solution 0.1% (Figure 9). After 2 hours, the permeability was tested again on the same 4 specimens, if the permeability remained the same all 20 specimens were maintained for two more hours in peroxide solution. On the other hand, if the permeability increased for at least two out of the four tested specimens, the 4 specimens were tested for compressive strength. The remaining specimens were placed on the reservoir with the activated sludge loaded water for longer time. This was repeated until all 20 specimens were tested for permeability and compressive strength.

Figure 9. PCPC specimens (C-2 design) in reservoir with 0.1% H_2O_2 solution

5. Results and Discussion

5.1 Cementitious Pastes

The consistency of fresh paste and setting time was compared using four cementitious pastes design with the different combination of materials. The four combinations were: Portland cement only (P-1), Portland cement with partial substitution by FA (P-2), Portland cement with $ENP_{Fe\text{-}surf}$ (P-3), and Portland cement partially substituted by FA and $ENP_{Fe\text{-}surf}$ (P-4). The short-term chemical exposure was done for the assessment of possible iron leaching behavior. Durability when exposed to acid attack was assessed for the four cementitious pastes using acetic acid and sulfuric acid.

5.1.1 Cementitious Paste Spread Percentage and Setting Time

Cement mortars are typically designed to have a spread percentage of 110 ± 5% (Jimenez-Quero et al., 2013). A particular value was not found for cement paste in the literature; nevertheless, this value was chosen in order to base the cementitious paste comparison. By taking the paste with only Portland cement and water as reference one can observe in Table 11 that by adding FA (no nanoparticles) the consistency of the mixture (P-2) decreased, when the water-to-binder ratio remained the same. Fly ash has smaller particle size and greater surface area, consequently requires more water for hydration. On the other hand the addition of $ENP_{Fe\text{-}surf}$ (P-3) increased the consistency. The paste with both FA and $ENP_{Fe\text{-}surf}$ (P-4) had lower the spread percentage than that with only cement, but it had a greater spread percentage than the paste (P-2).

Table 11. Flow table percentages of spread tested with a flow table

Percentage of Spread (%)				
Sample	$D_{f,1}$ (cm)	spread %	$D_{f,2}$ (cm)	spread %
P-1	21.2	112	21	110
P-2	18	80	15.2	52
P-3	23.4	134	23.9	139
P-4	19	90	17.6	76

*D_i = 10 cm

The setting time was also compared and the results are shown in Figure 10. The initial and final setting time are shown in Table 12 for each paste. Compared to the reference paste (i.e., cement only paste), the addition of FA and $ENP_{Fe\text{-}surf}$ (P-4) delayed the hardening process. The slowest setting time was observed for the paste P-3. Aydin et al. (2007) observed a delayed setting time with partial substitution by FA, but did not report the magnitude of the delay. Surfactants were utilized as water reducers and set retarders (Mehta and Monteiro, 2013). The $ENP_{Fe\text{-}surf}$ used in this research had a surfactant that maintains the nanoparticles disperse. The nanoparticles are proprietary by the Ferrotec and therefore the chemical composition of the surfactant is unknown. It is possible that the surfactant was responsible for increasing the spread percentage and the setting time of the cementitious mixture and not the nanoparticle. Other nanoparticles have been used and found to accelerate setting time opposed to $ENP_{Fe\text{-}surf}$. Nanoparticles of $CaCO_3$ (5%) were capable of accelerating setting time of cementitious pastes that had 50% of its cement replaced by FA (Kawashima et al., 2013). The $CaCO_3$ nanoparticle utilized was a dry powder, probably without a surfactant, which further supports the assumption that the delays in setting time observed was due to the surfactant present in the $ENP_{Fe\text{-}surf}$ solution.

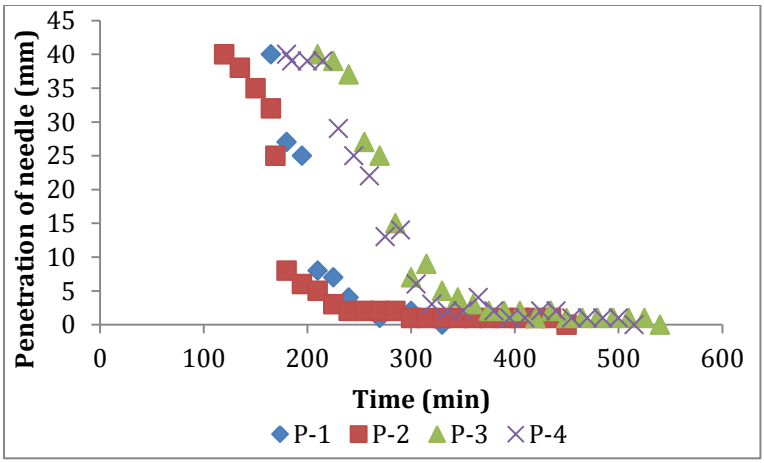

Figure 10. Setting time for all four cementitious pastes

Table 12. Setting time for each cementitious pastes

	Setting Time	
Mixture	Initial time	final time
P-1	195	330
P-2	169	450
P-3	270	540
P-4	245	515

[a]Initial time is when the needle penetrates 25 mm the paste

[b]Final time is when the needle does not penetrates the paste

5.1.2 Short-term Chemical Exposure

The short-term chemical resistances of the cementitious pastes were compared using three different solutions. Deionized water was used as the reference when compared to sulfuric acid and sodium chloride solutions. The deionized water pH where the paste specimens were placed remained to be 12 for all four combinations. The sodium chloride solution's pH also remained at 12 for all four cementitious pastes. On the other hand, the pH for the sulfuric acid solution began at 12 but decreased to 4 on the 9th day for all cementitious pastes. The pH behavior can be seen in Figure 11, Figure 12 and Figure 13.

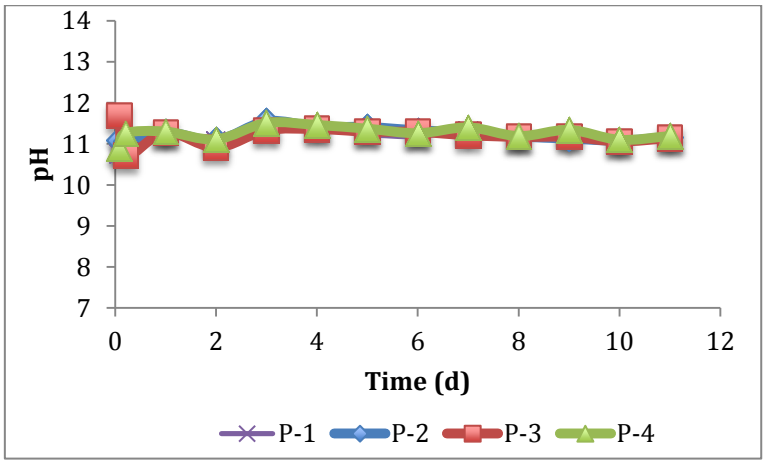

Figure 11. Water pH versus time for all four cementitious pastes in deionized water

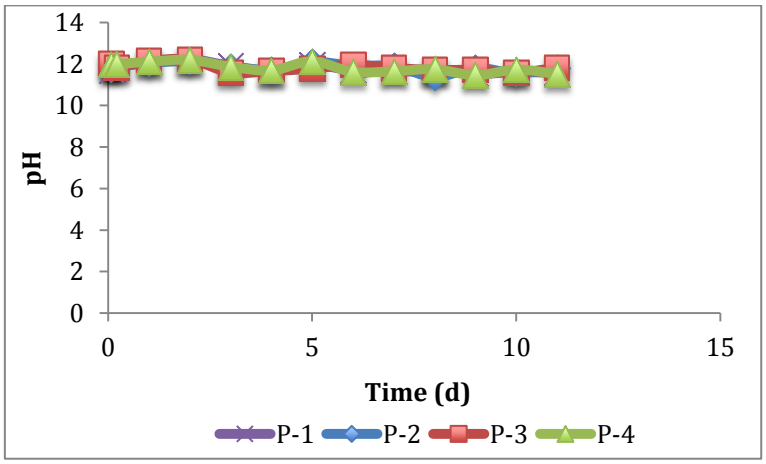

Figure 12. Solution pH versus time for all four cementitious pastes in sodium chloride solution (5% w/v)

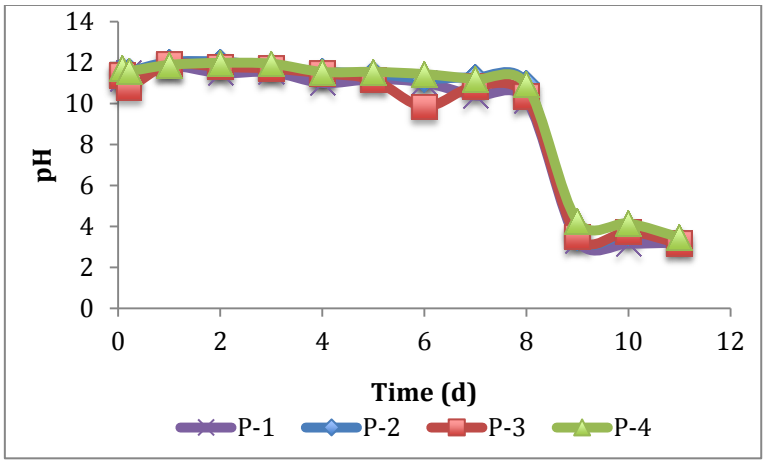

Figure 13. Solution pH versus time for all four cementitious pastes in sulfuric acid solution (0.01% v/v)

The iron concentration was also measured in order to assess possible iron leaching from the cementitious pastes. The iron concentration remained below the detection limit for all specimens placed in deionized water (Figure 14). For the other two solutions the iron concentration was sometimes above the minimum detection limit, although it remained below 0.08 mg/L. In the sodium chloride solution, the iron concentration did not follow a pattern (Figure 15), but in the sulfuric acid solution, it was above than minimum detectible limit after day 5. On the 9^{th} and 10^{th} day the iron concentrations were the highest in the sulfuric acid solution (Figure 16). It seemed that most of the iron stayed within the cementitious matrix.

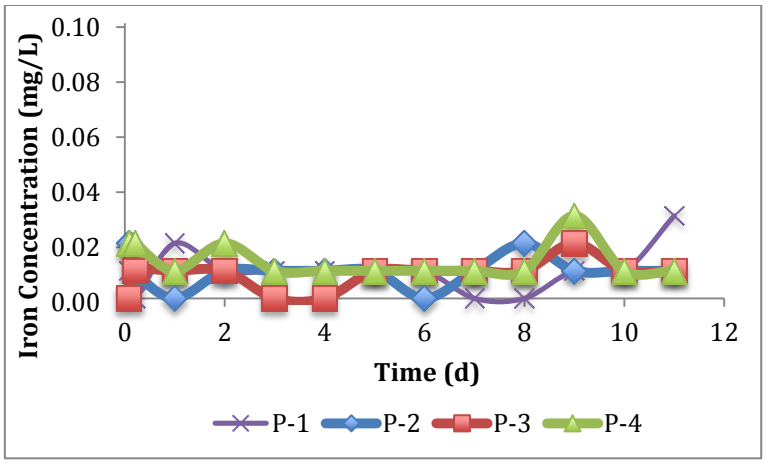

Figure 14. Iron concentration versus time for all four cementitious pastes in deionized water

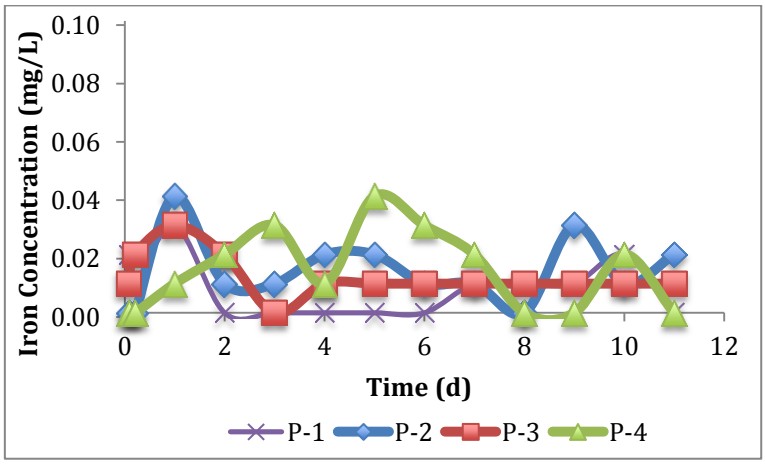

Figure 15. Iron concentration versus time for all four cementitious pastes in sodium chloride solution (5%w/v)

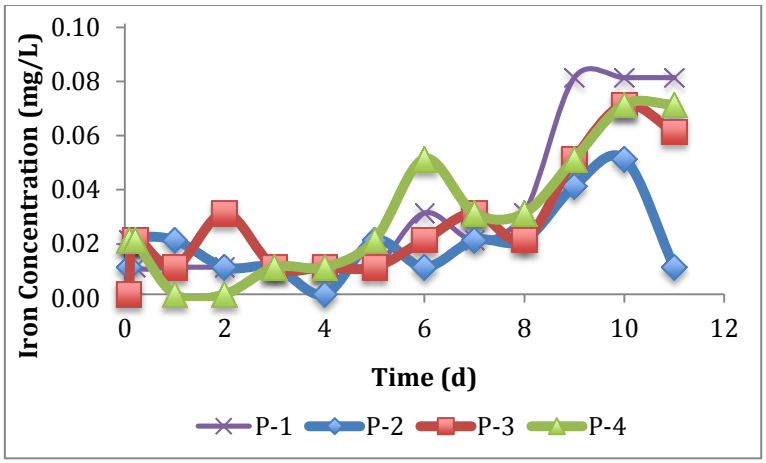

Figure 16. Iron concentration versus time for all four cementitious pastes in sulfuric acid solution (0.01% v/v)

The compressive strength values of each specimen measured after short-term chemical exposure are given in Table 13. The cementitious paste P-4 was the specimen that showed the highest compressive strength for each solution. The paste P-1 had the second highest compressive strength for deionized water and sodium chloride solution, but had the same compressive strength that the cementitious paste P-4 had. The cementitious pastes P-2 or P-3 had lower compressive strength compared to the cement only paste. The paste P-3 in acidic solution had the lowest compressive strength and was 55% lower when compared to P-1.

Table 13. Compressive strength (MPa) of each of the four cementitious pastes placed in each solution

Sample	Solutions		
	DI Water	H_2SO_4	NaCl
P-1	64.33	63.91	57.05
P-2	55.61	29.30	30.47
P-3	57.40	28.85	34.40
P-4	64.98	63.91	71.26

5.1.3 Long-term Acid Attack

Figure 17 shows the pH of the sulfuric solution that contained the specimens. The low pH at the beginning was possibly due to calcium hydroxide consumption being faster than its leaching from the corresponding specimen. The high pH values at a later time were possibly due to a complete neutralization of the sulfuric acid by calcium hydroxide in the solution.

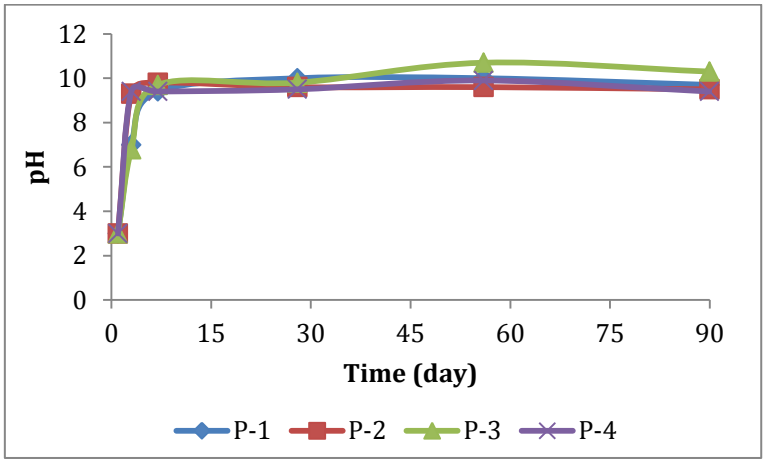

Figure 17. pH values for sulfuric acid solution versus time

The weight gain was obtained by comparing the mass measured on days 3, 7, 28, 56, and 90 to that on day 1. The specimens exposed to sulfuric attack for 90 days experienced a little weight gain between 0.23 and 0.46% after 90 days (Figure 18). While the specimens with FA (P-2 and P-4) started to gain weight immediately, those without FA (P-1 and P-3) had a lag phase in weight gained. It is believed that the specimens with FA had weight gained related to the reaction between FA and calcium hydroxide at the beginning of the experiment, along with the reactions related to acid or sulfate attack. Furthermore it can be infer that the sulfate and acid attack started between 7 and 28 days. All specimens exposed to sulfuric acid experience a weight gain up until 56 days, except for the specimen with Portland cement only (P-1). The specimen

P-2 experienced weight loss after 56 days. The two specimens with $ENP_{Fe\text{-}surf}$ (P-3 and P-4) maintained a constant weight gain between 56 and 90 days.

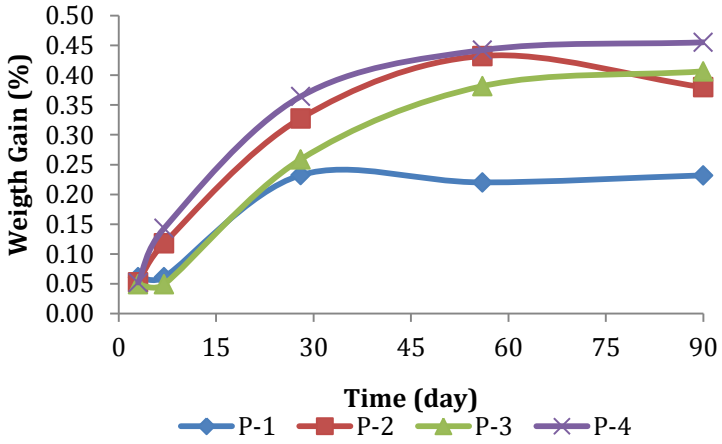

Figure 18. Weight gained by specimens exposed to sulfuric acid (initial pH 3) versus time

Weight gain can be attributed to three processes: (1) further hydration of cement, (2) production of expansive reaction products such as gypsum and ettringite and (3) water absorption. On the other hand weight loss is attributed to dissolution of cementitious material, mainly calcium hydroxide (Makhloufi, et. al, 2012). Hossain and Lachemi (2006) measured marginal weight gain, which was lower for the specimens with natural pozzolans (volcanic ash and volcanic pumice) than the specimens with either Type I or Type V cement. On the other hand, Makhloufi et al. (2012) measured higher weight gaining in specimens with higher portions of slag or natural pozzolana.

Based on these findings one can say that the FA used in the current study, like either the slag or the natural pozzolana used by Makhoufi, promoted further production of C-S-H gel, production of expansive reaction products and consumption of calcium hydroxide. Probably after 56 days the specimens P-2 produce more expansive products quicker than the dissolution of calcium hydroxide. But after 56 days this production decreased and the dissolution increased. Li

(2004) has measured a decrease in pore size for concrete specimens with high volume of FA and SiO_2 nanoparticles, which was attributed to nucleating site effect. It is possible that the addition of $ENP_{Fe\text{-}surf}$ in the presence of sulfate ions is facilitating the formation of iron-substituted ettringite and iron-substituted monosulfate hydrate, both expansive reaction products. The formation of both expansive reaction products will eventually damage the cementitious paste by cracks formation. Further study is needed to identify the compound produced due to the presence of $ENP_{Fe\text{-}surf}$.

The pH of the acetic solution did not reach such high pH values as the sulfuric solution did, as can be seen in Figure 19. Its increment was slower and it decreased and stayed below 7 after 56 days. It is possible that this behavior occurred due to a higher concentration of acetic acid compared to sulfuric acid. The calcium hydroxide was consumed by the higher acetic acid concentration. Both specimens that had 40% of Portland cement substituted by FA (P-2 and P-4) did not experience an increase in pH as the other two. It is possible that this occurred due to partial consumption of calcium hydroxide by FA prior to the specimens being exposed to the acetic acid solution. Bertron et al. (2005b) observed pH values between 11 and 12 for an organic acid solution (acetic acid and other organic acids) and calcium concentration in the solution that reached a maximum and then decreased. The researchers crushed the samples prior to exposure to organic acid solution, which could have facilitated calcium leach, even after pozzolanic reaction.

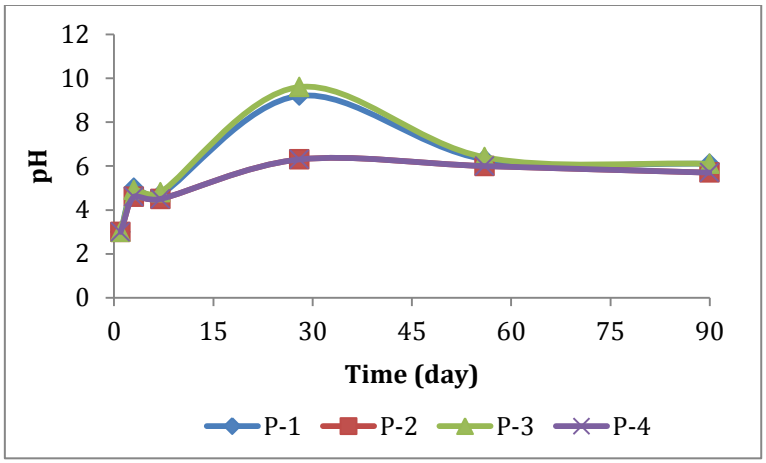

Figure 19. pH of acetic acid solution versus time

The specimens exposed to acetic acid experienced a weight loss throughout the 90 days period of time (Figure 20). The weight loss ranged between 2.7% and 3.2%. The specimen with the lowest weight loss was P-3; highest was P-2. The addition of $ENP_{Fe\text{-}surf}$ to the cementitious paste helps decrease weight loss for the specimens with partial Portland cement substitution by FA.

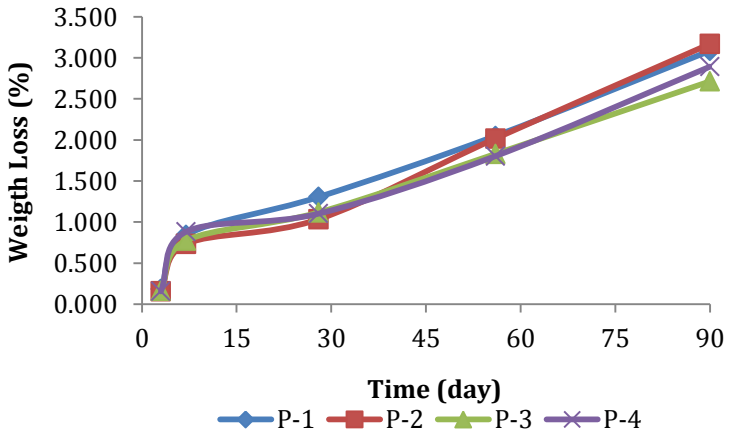

Figure 20. Weight gained by specimens exposed to acetic acid (initial pH 3) versus time

Bertron et al. (2005a) also observed a mass loss in cementitious pastes. They compared cementitious pastes (with and without blast-furnace slag) that were exposed to a mixture of organic acid (including acetic acid) at initial pH of either 4 or 6. They found that the specimens with blast-furnace slag had the lowest mass loss and that the specimens exposed to higher initial pH values had a higher mass loss. This was in line with our research that showed higher mass losses at higher initial pH. Bertron et al. (2005a) attributed the mass loss to decalcification. As previously mentioned, the weight loss is related to the dissolution of calcium hydroxide. As the samples with $ENP_{Fe\text{-}surf}$ added have a lower weight loss it seemed that the nanoparticles were promoting the production of C-S-H gel or other compound other than calcium hydroxide. Another possibility is that the $ENP_{Fe\text{-}surf}$ produced a smaller pore size in the cementitious paste, which slowed down the dissolution of calcium hydroxide. Further research is needed in order to test this possibility.

The surface texture and visual appearance of the specimens exposed to acetic and sulfuric acid were different from each other. The specimens in acetic acid were mushy and soft. On the other hand, the specimens exposed to sulfuric acid seemed hard after 90 days. The specimens exposed to sulfuric acid for 7 and 90 days are shown in Figure 21 and Figure 22, respectively. The specimens exposed to acetic acid for 7 and 90 days are shown in Figure 23 and Figure 24, respectively.

Figure 21. Cementitious pastes exposed to sulfuric acid for 7 days: a) 0%FA/B and 0% ENP/B, b) 0%FA/B and 3% ENP/B, c) 40%FA/B and 0% ENP/B, and d) 40%FA/B and 3% ENP/B.

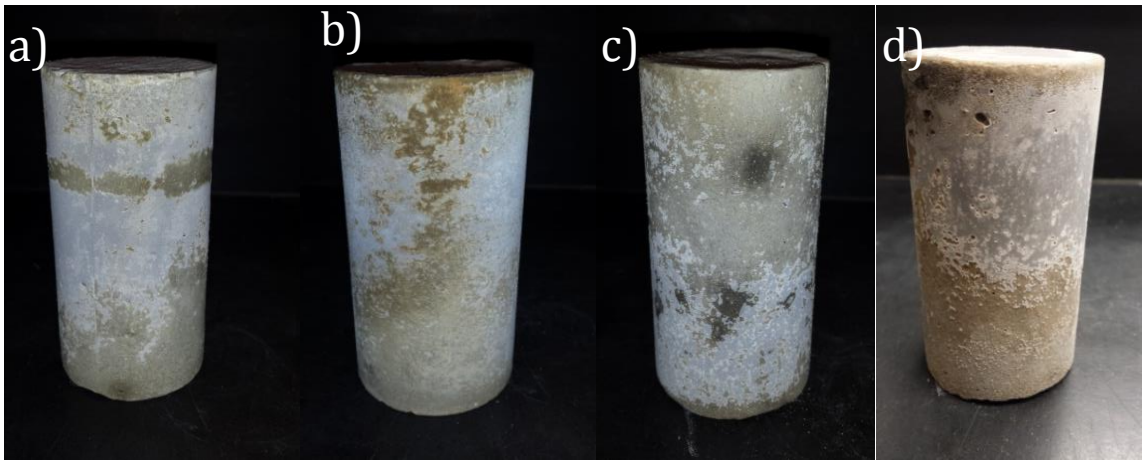

Figure 22. Cementitious pastes exposed to sulfuric acid for 90 days: a) 0%FA/B and 0% ENP/B, b) 0%FA/B and 3% ENP/B, c) 40%FA/B and 0% ENP/B, and d) 40%FA/B and 3% ENP/B.

Figure 23. Cementitious pastes exposed to acetic acid for 7 days: a) 0%FA/B and 0% ENP/B, b) 0%FA/B and 3% ENP/B, c) 40%FA/B and 0% ENP/B, and d) 40%FA/B and 3% ENP/B.

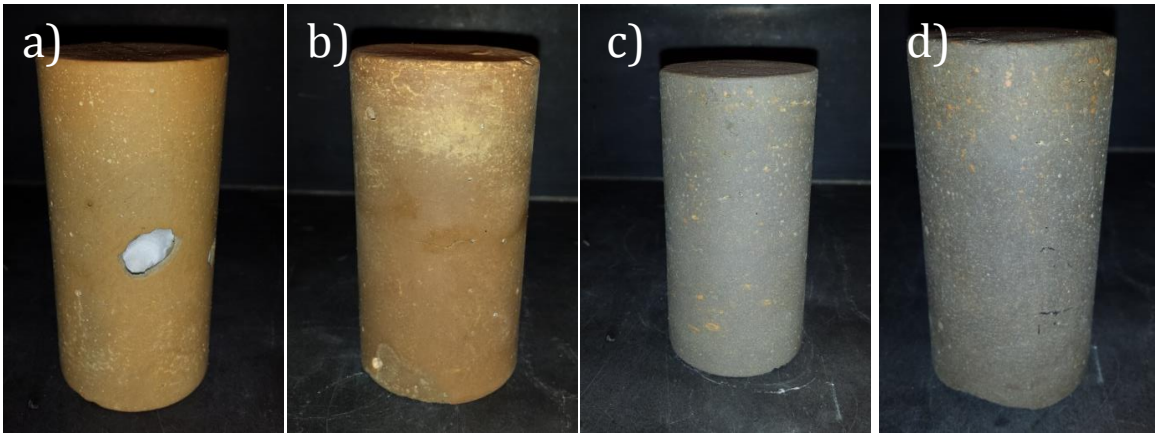

Figure 24. Cementitious pastes exposed to acetic acid for 90 days: a) 0%FA/B and 0% ENP/B, b) 0%FA/B and 3% ENP/B, c) 40%FA/B and 0% ENP/B, and d) 40%FA/B and 3% ENP/B.

After the 90 days, the specimens were tested for compressive strength and the values obtained are shown in Table 14. The specimens under acetic acid attack were weaker than the ones under sulfuric acid attack, which coincided with the surface texture and visual appearance aforementioned. It has been mentioned in the literature that organic acids usually degrade more cementitious paste than strong acid when compared at a given pH value due to the organic acid's higher concentration (Gruyaert et al., 2012). Coincidently in general specimens exposed to sulfuric had better mechanical properties than the specimens exposed to acetic acid. This is possible because the specimens exposed to sulfuric acid had expansive reaction products that formed in the pores left by the consumed calcium hydroxide, in contrast to the specimens exposed to acetic acid. The specimens with only Portland cement (P-1) had the highest compressive strength followed by the ones with $ENP_{Fe\text{-}surf}$ (P-3). The specimens with partial substitution of Portland cement by FA (P-2 and P-4) obtained the lowest compressive strength. But it was observed that the addition of $ENP_{Fe\text{-}surf}$ to the FA-Portland cement cementitious matrix contributes to its compressive strength.

Table 14. Compressive strength of cementitious pastes after 90 days in acidic solutions

FA/B (%)	ENP/B (%)	Acetic Acid		Sulfuric Acid	
		(MPa)	Avg. (MPa)	(MPa)	Avg. (MPa)
0	0	62.40 66.81	64.60	63.26 79.05	71.15
0	3	51.23 62.36	56.80	68.05 74.12	71.08
40	0	40.99 42.30	41.64	42.51 49.37	45.94
40	3	48.44 41.16	44.80	44.61 57.36	50.99

5.2 Portland Cement Pervious Concrete

Response Surface Methodology (RSM) is a statistical model used to assess the influence of different variables and interactions on a response of interest. The software Minitab 16.1 was utilized in order to develop the RSM. The combinations of all three factors and the results obtained for each mixture are shown in Table 15.

Table 15. Combination factors and their responses

Standard Order	W/B Ratio (%)	FA/B Ratio (%)	ENP/B Ratio (%)	Compressive Strength (MPa)	Permeability (mm/s)	Void Content (%)	Density (kg/m^3)
1	34.0	10.0	1.0	11.32	10.75	15.8	2266.7
2	40.0	40.0	1.0	10.29	7.62	12.8	2299.6
3	40.0	10.0	5.0	11.38	12.09	15.9	2246.7
4	34.0	40.0	5.0	7.81	12.52	17.2	2217.4
5	37.0	25.0	3.0	10.93	5.98	14.3	2283.0
6	37.0	25.0	3.0	7.08	11.98	16.6	2231.2
7	40.0	10.0	1.0	11.27	6.77	12.8	2296.0
8	34.0	40.0	1.0	7.05	15.18	19.2	2175.4
9	34.0	10.0	5.0	11.62	8.24	14.8	2286.0
10	40.0	40.0	5.0	9.58	7.74	13.1	2280.4
11	37.0	25.0	3.0	10.65	7.29	12.5	2314.8
12	37.0	25.0	3.0	10.38	7.42	11.9	2335.0
13	32.1	25.0	3.0	3.45	15.76	20.6	2136.6
14	41.9	25.0	3.0	6.45	6.32	10.9	2318.4
15	37.0	0.5	3.0	12.81	6.63	11.8	2337.2
16	37.0	49.5	3.0	3.50	9.55	14.5	2272.5
17	37.0	25.0	0.3	6.41	8.15	13.0	2308.9
18	37.0	25.0	6.3	7.91	7.28	11.3	2342.3
19	37.0	25.0	3.0	6.60	8.98	15.0	2265.2
20	37.0	25.0	3.0	5.77	9.44	14.2	2281.5
21	34.0	10.0	1.0	8.60	7.84	14.9	2312.7
22	40.0	40.0	1.0	8.20	5.31	13.5	2320.0
23	40.0	10.0	5.0	13.07	5.38	10.8	2357.8
24	34.0	40.0	5.0	6.67	9.05	16.6	2271.0
25	37.0	25.0	3.0	10.81	8.25	16.3	2251.0
26	37.0	25.0	3.0	9.57	9.12	17.3	2243.3
27	40.0	10.0	1.0	11.79	6.21	12.5	2300.4
28	34.0	40.0	1.0	6.34	16.79	20.4	2141.3
29	34.0	10.0	5.0	12.62	11.98	17.4	2207.2
30	40.0	40.0	5.0	10.14	7.38	13.1	2295.1
31	37.0	25.0	3.0	13.46	9.30	14.9	2258.6
32	37.0	25.0	3.0	12.07	6.54	13.3	2316.9
33	32.1	25.0	3.0	4.27	17.40	22.2	2121.6
34	41.9	25.0	3.0	11.86	7.50	13.6	2298.4
35	37.0	0.5	3.0	10.34	7.27	13.1	2338.9
36	37.0	49.5	3.0	2.50	11.97	17.6	2190.8
37	37.0	25.0	0.3	6.22	12.06	17.6	2221.6
38	37.0	25.0	6.3	11.22	7.20	12.5	2320.2
39	37.0	25.0	3.0	7.91	12.50	22.2	2230.7
40	37.0	25.0	3.0	8.46	10.34	15.6	2269.3

Using the results from the RSM, a matrix plot was developed in Minitab 16.1 for the Pearson's correlations shown in Figure 25 and Table 16, respectively. In Table 16 the first number is the r-value, which indicates the strength and direction of the correlation. The number underneath the r-value is the p-value. If it is lower than 0.05, then the correlation is accepted. Permeability and void content had a direct (or positive) correlation; on the other hand permeability and density had an inverted (or negative) correlation. The void content and density had an inverse correlation. It is construed that as the void content increases the chances of those void spaces being interconnected increases consequently increasing the permeability. Since all mixtures were prepared with the same amount of gravel, it is believed that the increase of void content was due to a decrease in the amount of cementitious paste. The compressive strength did not have a strong correlation with the other variables, but there still was an inverse correlation with permeability and void content, and a direct correlation with the density.

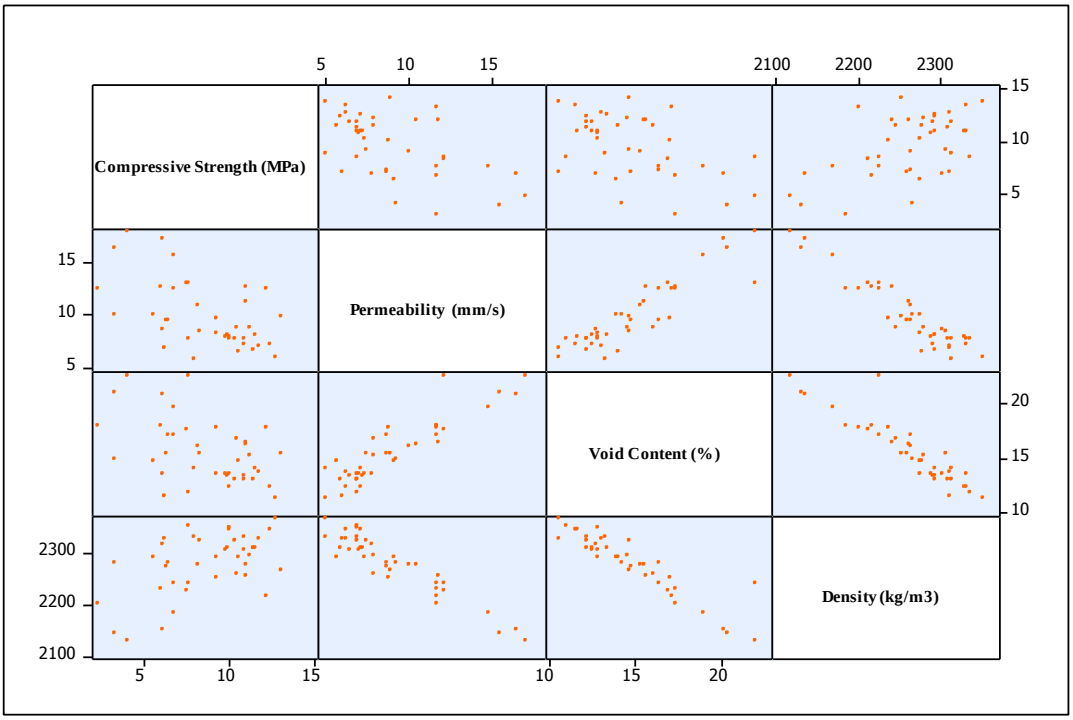

Figure 25. Matrix plot for compressive strength, permeability, void content and density of hardened PCPC

Table 16. Pearson's correlations for each response

Correlations			
	Compressive Strength (MPa)	Permeability (mm/s)	Void Content (%)
Permeability (mm/s)	-0.548 0.000		
Void Content (%)	-0.490 0.001	0.900 0.000	
Density (kg/m^3)	0.537 0.000	-0.940 0.000	-0.920 0.000

Using the second order model described in the Literature Review section, the regression values were estimated for each response. Estimated regression values for compressive strength, permeability, void content, and hardened density are given in equations 10 to 13, where W/B, FA/B, and ENP/B variables are the coded values. The R^2 values for compressive strength, permeability, void content and density of hardened concrete were; 81.1, 80.9, 79.9, and 73.9%, respectively.

$$Compressive\ Strength = 9.47 + 1.16\frac{W}{B} - 2.01\frac{FA}{B} + 0.70\frac{ENP}{B} \quad (10)$$

$$Permeability = 8.92\ - 2.45\frac{W}{B} - 0.93\frac{FA}{B} + 0.96\left(\frac{W}{B}\right)^2 - 1.07\frac{W}{B}\frac{FA}{B} + 0.97\frac{W}{B}\frac{ENP}{B} - 0.90\frac{FA}{B}\frac{ENP}{B} \quad (11)$$

$$Void\ Content = \ 14.94 - 2.31\frac{W}{B} + 0.85\frac{FA}{B} + 0.76\left(\frac{W}{B}\right)^2 \quad (12)$$

$$Density = 2273.08 + 41.40\frac{W}{B} - 23.28\frac{FA}{B} - 20.58\left(\frac{W}{B}\right)^2 \quad (13)$$

The statistical model contains only the terms that are statistical relevant i.e. those with P-value less than 0.05 (Appendix A). The standard residuals of all four responses were utilized to verify normality, equal variance and independence, shown in Appendix B.

5.2.1 Contour Plots from RSM

Using the statistical model, response surface graphs and contour plots were obtained for compressive strength, permeability, void content and density of hardened concrete. The response surface graphs and some contour plots are in Appendix C. As the iron oxide nanoparticles had least statistical influence in the responses or none at all it was decided to present the contour plots keeping the ENP/B ratio constant (3 or/and 5%).

The reduction in FA/B ratio had a greater influence on compressive strength than the increase in either W/B or ENP/B. The compressive strength did not have variables with quadratic influence or interactions. Remembering that FA develops compressive strength at long term, one can choose a minimum compressive strength, for example 10.00 MPa, and see how much one can increase the FA/B ratio. The highest value of FA/B would be 25 as shown in Figure 26 and Figure 27. The W/B had a positive sign implying, within the chosen range, that it was better to increase the water content in order to increase the compressive strength. The nanoparticles addition had the lesser influence on compressive strength, although it can be used to increase the FA/B ratio as can be seen in Figure 26 and Figure 27 that had ENP/B ratio kept at 3 and 5%, respectively.

Other researchers have studied the increment of compressive strength in cement pastes and in concrete associated to the addition of nanoparticles such as TiO_2, Fe_2O_3, Al_2O_3 and SiO_2 (Khoshakhagh et al., 2012; Li, 2004; Nazari and Riahi, 2011 Otulu and Sahin, 2013). The

increase in compressive strength by the nanoparticle presence was attributed to nanoparticle acting as nano-filler reducing the size of pore in the cement paste (Khoshakhagh, et al., 2012; Li, 2004). In the case of PCPC, the increase of strength of the cementitious paste would benefit the material as the paste is usually weaker than the aggregates.

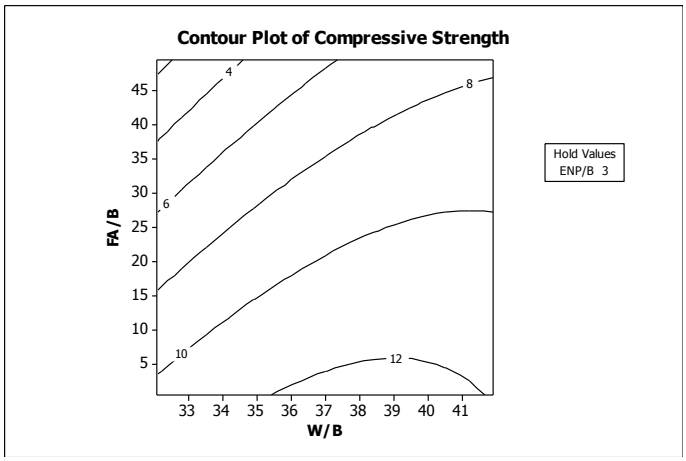

Figure 26. Contour plot for compressive strength maintaining ENP/B ratio at 3%

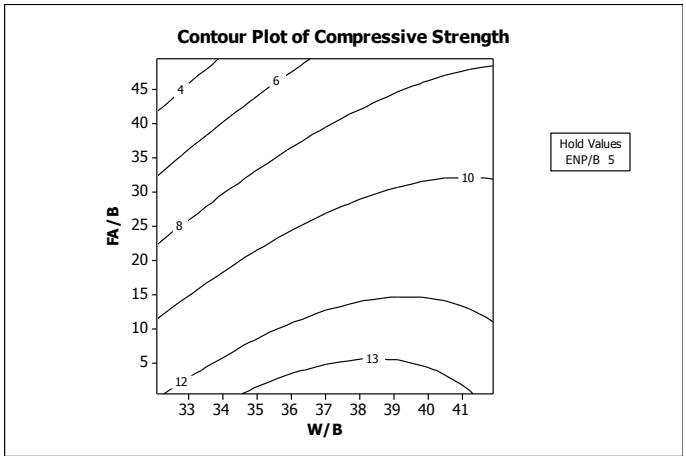

Figure 27. Contour plot for compressive strength maintaining ENP/B ratio at 5%

The permeability had linear and quadratic influence and was involved in interactive effects. The W/B ratio had both linear and quadratic effect on the model and had the highest influence on the permeability followed by the W/B*FA/B and W/B*ENP/B interactions. Contrary to

compressive strength, in order to increase the permeability the W/B ratio had to be decreased and the FA/B ratio increased (Figure 28). It is believe that because FA requires more water due to smaller particle size and higher surface area, as consequence the cementitious paste is less fluidic preventing the interconnected pores from being clogged by the paste. The ENP/B ratio had no statistical relevance on its own, although it was present as part of interactions. The $ENP_{Fe\text{-}surf}$ is coated with a surfactant in order to prevent the nanoparticles from clogging in the solution. As previously mentioned surfactant is used to increase workability, the surfactant coated on the $ENP_{Fe\text{-}surf}$ could be responsible for the interactive effect on the PCPC instead of the nanoparticle. If the cementitious paste in the PCPC is too high the paste can drip to the bottom (i.e., bleeding) resulting in decrease in the void content at the bottom and consequently the permeability. Chindaprasirt et al. (2008) did an inspection of the void content in the bottom layer and found that as the workability of the mixture increased the void content decreased. Therefore, it is assumed that if the $ENP_{Fe\text{-}surf}$ increased the workability or consistency of the fresh mixture possibly causing segregation. Therefore the specimens with higher ENP/B ratios would have had less permeability due to lesser void content at the bottom (Figure 28 and Figure 29). The highest value of permeability obtained was 17.4 mm/s (average), although 8.0 mm/s should suffice. This means that W/B and FA/B ratios can be chosen in order to obtain acceptable compressive strength and permeability values.

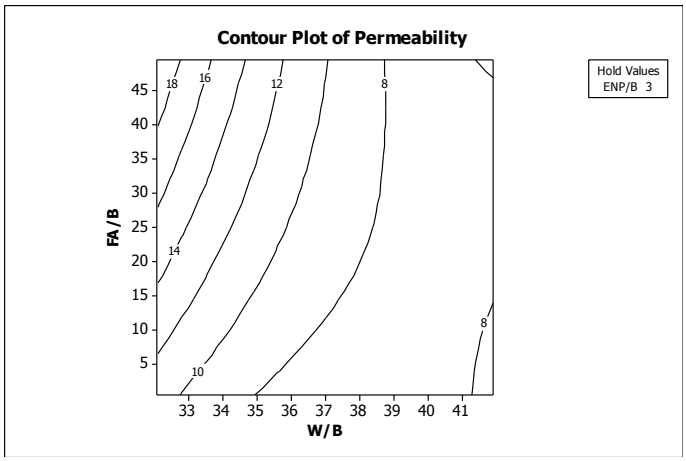

Figure 28. Contour plot for permeability maintaining ENP/B ratio at 3%

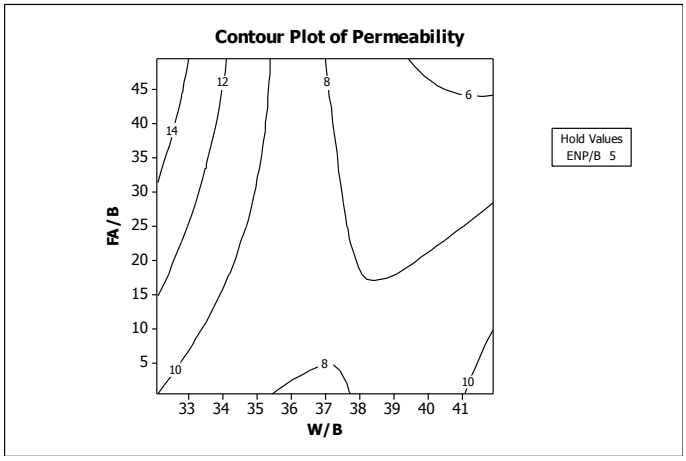

Figure 29. Contour plot for permeability maintaining ENP/B ratio at 5%

The variable W/B had a linear and a quadratic influence on the void content; on the other hand FA/B had a linear influence. In order to increase the void content the W/B ratio should be decreased and the FA utilization should be increased, as shown in Figure 30. The inverse relation between W/B and void content was also observed by Sonebi and Bassuoni (2013). Chindaprasirt et al. (2008) has studied the inverse relation between void ratio and compressive strength and found that both responses could not be increased at the same time. This was due to concentration

of stress and crack formations in the void present in the concrete matrix when the PCPC is under a load.

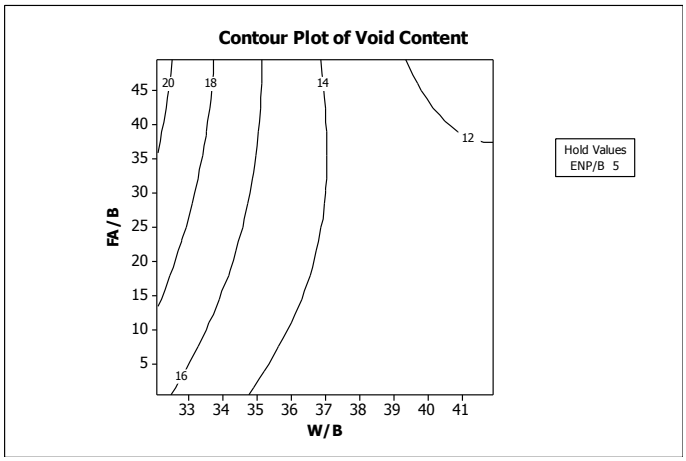

Figure 30. Contour plot for void content maintaining ENP/B ratio at 5%

Density, like void content was influenced by W/B ratio (linear and quadratic) and the FA/B ratio. The W/B had the greatest influence on the density of hardened concrete. If the W/B was increased the density increased, similar to compressive strength. Ibrahim et al. (2014) found that the compressive strength increased linearly with the density. A greater density signifies a greater amount of cementitious paste and consequently less void space, decreasing the void content and increasing compressive strength. The increase of FA utilization decreased the density, as can be seen in Figure 31. This was due to the fact that FA had a lower specific gravity than Portland cement. The nanoparticles addition did not have a statistical significance for this response.

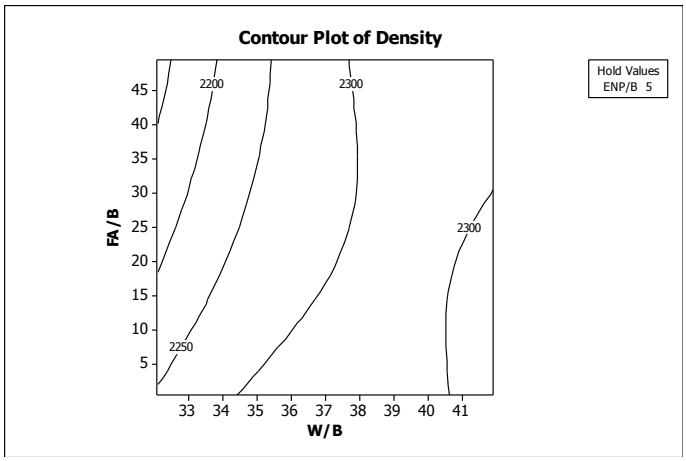

Figure 31. Contour plot for density of hardened concrete maintaining ENP/B ratio at 5%

All four responses were combined in order to obtain a contour plot that can show an area with desired optimum values for all responses. The compressive strength is desired to be 10 MPa or higher. The permeability and void content should be within the ranges of 8 and 14 mm/s, and 15 and 20%. The density was maintained between 2200 and 2300 kg/m^3 in order to accommodate all other responses desirable ranges as this is the response with the least importance. By maintaining the ENP/B ratio constant at 3%, Figure 32 was obtained. It shows a small region (in white) in which smaller values of W/B and FA/B ratios can be utilized. When the ENP/B ratio was maintained constant at 5% one can see that the region increased (Figure 33). 34%, 15% and 5% were chosen for W/B, FA/B and ENP/B ratios, respectively, for optimum mixture design.

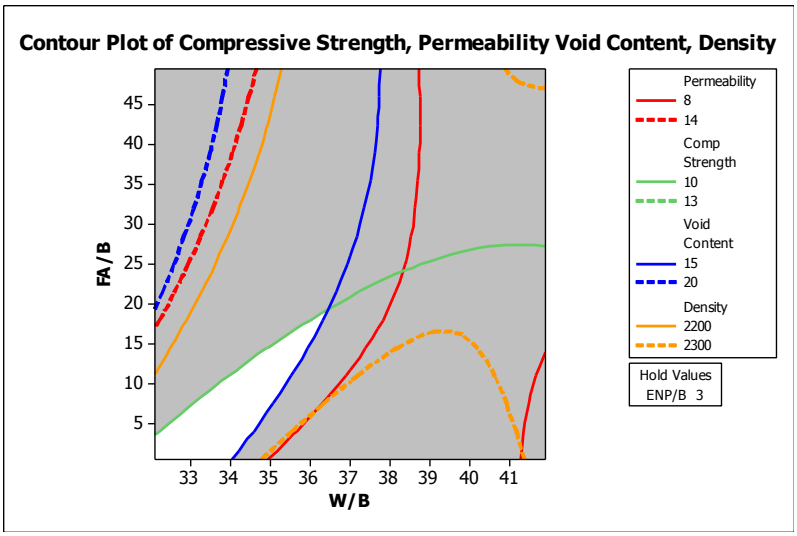

Figure 32. Overlaid contour plots for compressive strength, permeability, void content, and density of hardened concrete maintaining ENP/B ratio at 3%

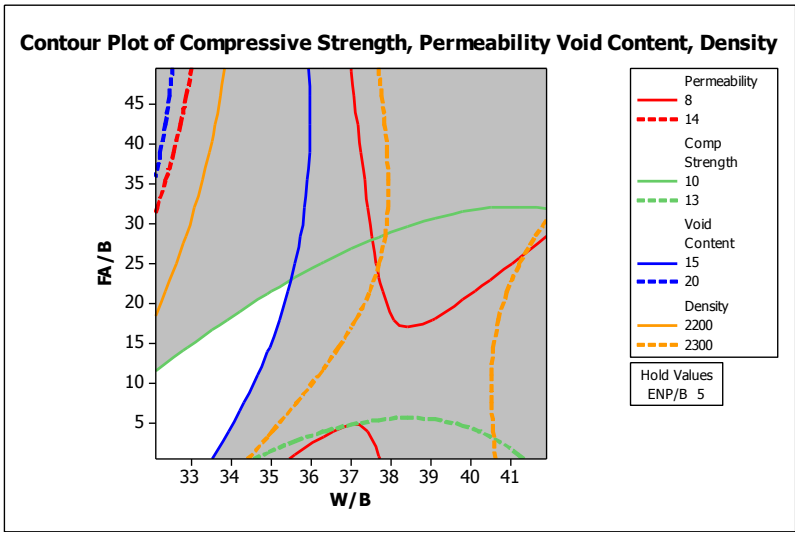

Figure 33. Overlaid contour plots for compressive strength, permeability, void content, and density of hardened concrete maintaining ENP/B ratio at 5%

5.2.2 Validation of Optimum PCPC Mixture

Using the optimum and the control designs PCPC specimens were tested for each response in order to validate the RSM optimization. The specimen with the optimization design

will be identified as Op for the remainder of this discussion. The compressive strength values shown in Table 17 were averaged and used to obtain the values used in Figure 34, Figure 35, Figure 36, and Figure 37. The compressive strength was expected to be over 10 MPa after 7 days of curing for the optimum design and to increase as curing time increased. However, the specimens with the optimum design did not reach the expected value. The some optimum samples reached 10 MPa after 28 days of curing. Chen et al. (2013) have observed a logarithmic increment in compressive strength as curing time increased regardless of its porosity. Although the optimum design did not reach expected values it showed a logarithmic behavior as can be seen in Table 17 and Figure 34. The PCPC specimens C-2 also followed a logarithmic increment, but C-1 and C-3 did not. This lack of logarithmic behavior can be due absence of FA.

Table 17. Compressive strength (MPa) for optimum and control PCPC designs at different curing time (d)

	Compressive Strength (MPa)				
Sample	3 days	7 days	28 days	56 days	90 days
C-1	7.55	11.07	7.93	9.17	8.69
	7.83	10.10	9.10	14.24	14.58
C-2	5.34	5.14	8.34	9.00	11.03
	5.07	7.79	9.31	12.96	11.34
C-3	6.89	10.89	10.41	11.96	9.76
	7.14	10.79	9.79	6.89	10.34
Op	7.10	8.00	8.55	9.96	11.82
	6.52	5.93	10.24	9.83	7.96

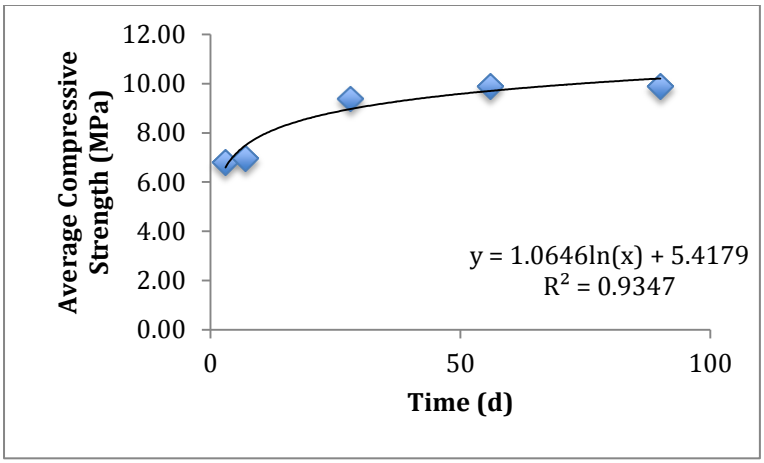

Figure 34. Average compressive strength for specimen Op

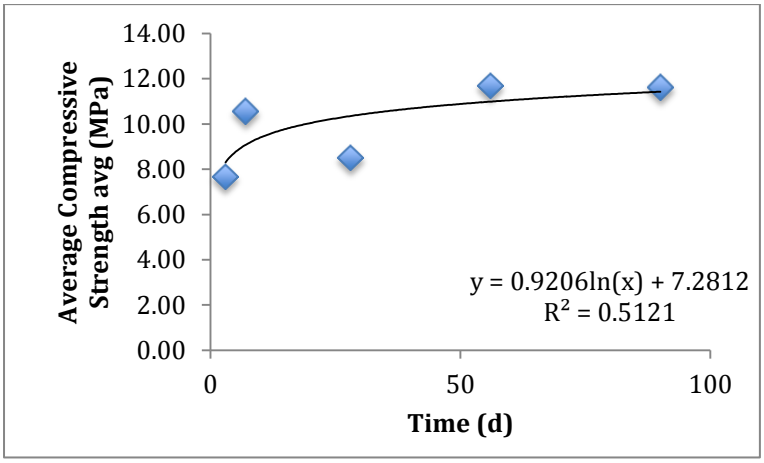

Figure 35. Average compressive strength for specimen C-1

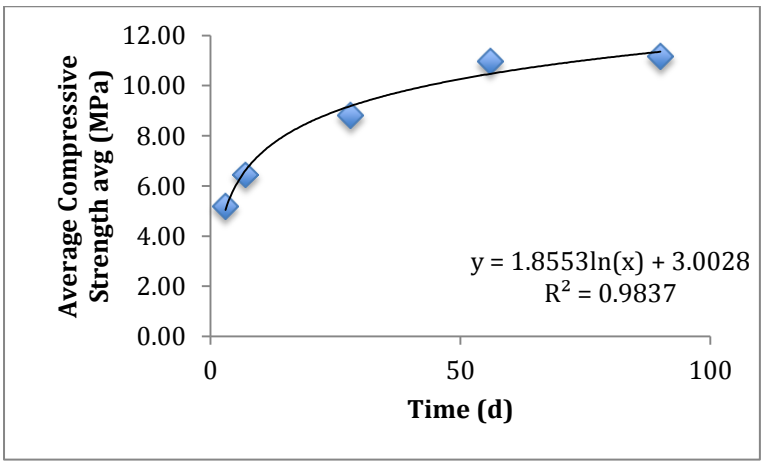

Figure 36. Average compressive strength for specimen C-2

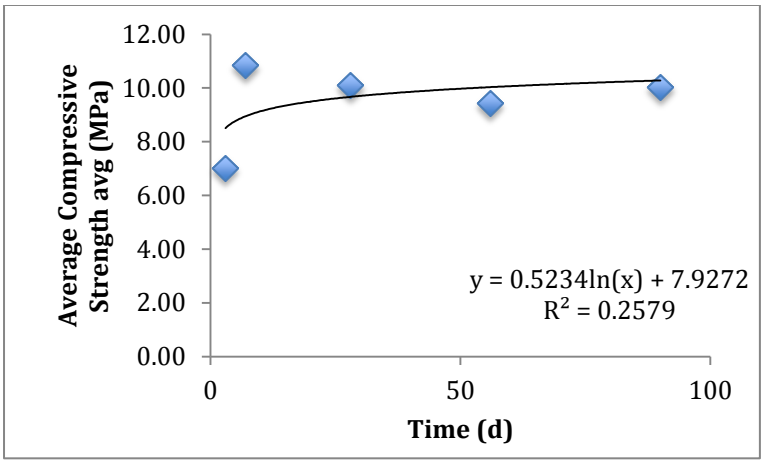

Figure 37. Average compressive strength for specimen C-3

As shown in Figure 38 where all four combinations were compared to each other, the specimens with only Portland cement and the specimens with $ENP_{Fe\text{-}surf}$ had greater compressive strength than the specimens with FA up to 28 days. Reportedly, the production of Portland cement is responsible for 5 to 8% of all man made CO_2 (Flatt et al., 2012). Consequently it is imperative to decrease its usage. After 56 days the specimens without $ENP_{Fe\text{-}surf}$ addition had higher compressive strength values, although no statistical difference was found after using t-test. This leads to the assumption that the Portland cement can be partially substituted when making PCPC, as there was no statistical difference between the two compressive strength values, although its use is limited by its low values. The addition of $ENP_{Fe\text{-}surf}$ increased the compressive strength at the beginning, although it decreased at later curing times. But once again there was no statistical relevance in the differences in compressive strength values.

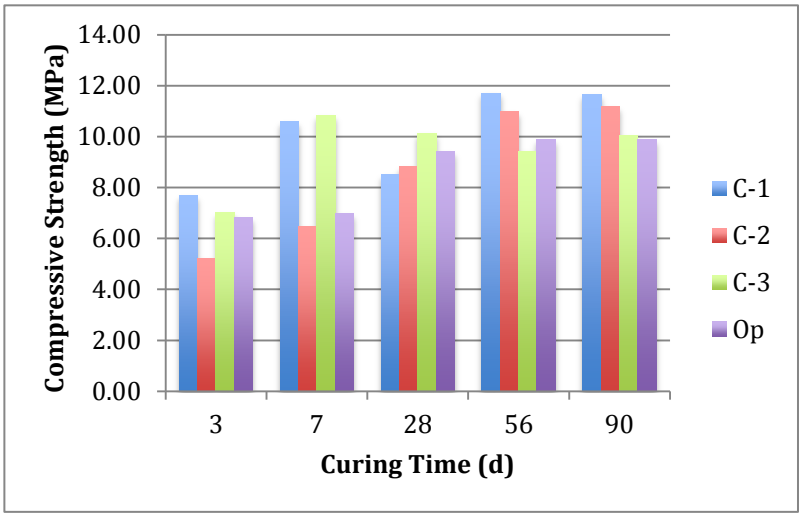

Figure 38. Compressive strength of all four PCPC specimens

Other researchers have incorporated nanoparticles in concrete and found that it increased the compressive strength with time. Li (2004) incorporated FA and SiO_2 nanoparticle to concrete specimens and found that the nanoparticles improved the compressive strength of the concrete after 150 days. This increment in compressive strength could be attributed to the observed reduction in pores within the cementitious matrix in the concrete specimens. Oltulu and Sahin (2013) compared the addition of nano-SiO_2, nano-Al_2O_3 and Fe_2O_3 to cementitious mortars containing FA (15% FA/B ratio) and found that all three nanoparticles increased the compressive strength although nano-SiO_2 showed the highest improvement. Although both studies were not with PCPC specimens it can be assumed that if the cementitious paste is improved, the PCPC specimen's compressive strength would be improved likewise. Further research is needed in which other nanoparticles are incorporated in PCPC in order to establish if the nanoparticle addition can or cannot improve its compressive strength.

The specimens were tested for void content, permeability and density. All measured values for the optimum design and controls are shown in Table 18. For the optimum design void

content, permeability and density values were within the established ranges. The optimum design had lower void content than the other control specimens, and the specimen C-2 had the highest void content. Similarly the optimum design specimens had the lowest permeability values and the specimen C-2 the highest. Using the values from Table 18, graphs were prepared to compare all three responses. As shown in Figure 39, the void content increased as the permeability increased. In Figure 40 and Figure 41 show decrease in the density as with decrease in the void content and the permeability. All three trends were observed regardless of the combination of materials used to prepare the PCPC specimens and were observed previously in the Matrix Plot in Figure 25.

Table 18. Void content, permeability and density of hardened PCPC specimens

Sample	Void Content (%)	Permeability (mm/s)	Density (kg/m^3)
C-1	17.8	11.5	2269.3
	18.9	12.6	2231.8
C-2	23.1	20.5	2118.7
	21.6	18.2	2165.1
C-3	22.3	18.8	2153.0
	18.5	12.5	2251.4
Op	16.2	11.0	2286.4
	17.9	12.9	2244.8

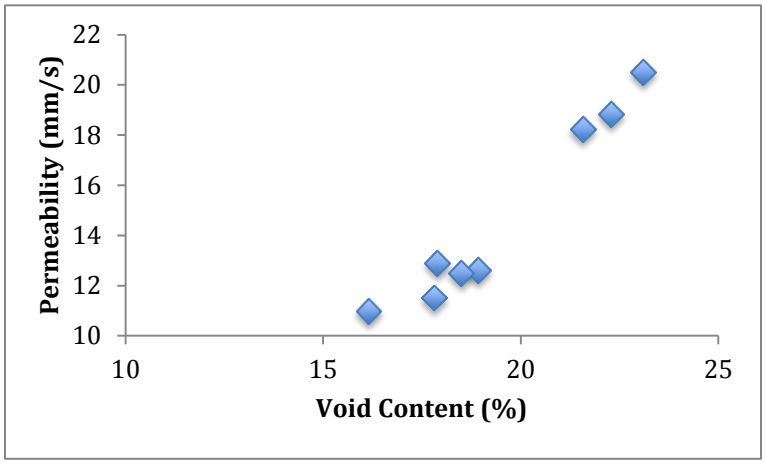

Figure 39. Permeability versus void content

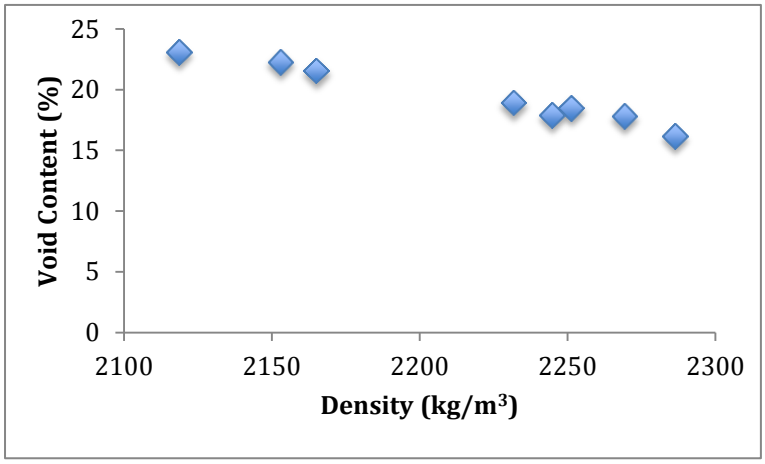

Figure 40. Void content (%) versus density of hardened PCPC

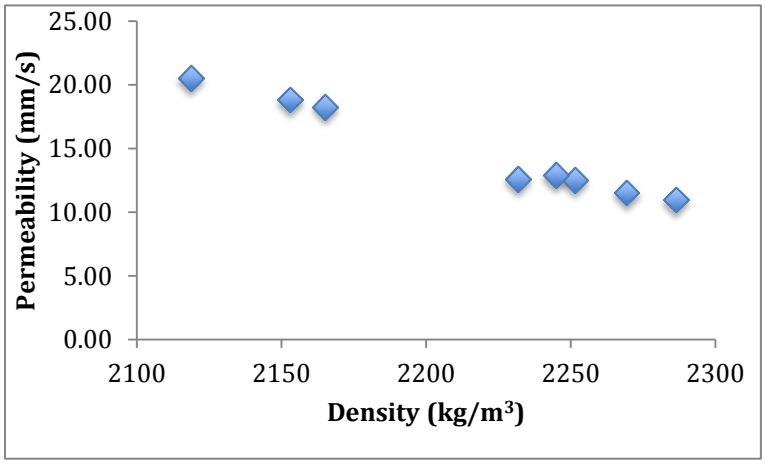

Figure 41. Permeability versus density of hardened PCPC

5.3 Iron Leaching from PCPC

The pH in the solution where optimum design mixture and the controls specimens were placed was measured to be 12. In Figure 42 is an example of the pH behavior for optimum design specimens. Other graphs are available in the Appendix. It is possible that the pH was around 12 due to $Ca(OH)_2$ leaching, although its measurement is beyond the scope of this research. The iron concentration remained below the minimum detection limit for all four specimens and was stopped after 12 days (Figure 43). The graphs of iron concentration for control specimens are available in the Appendix D.

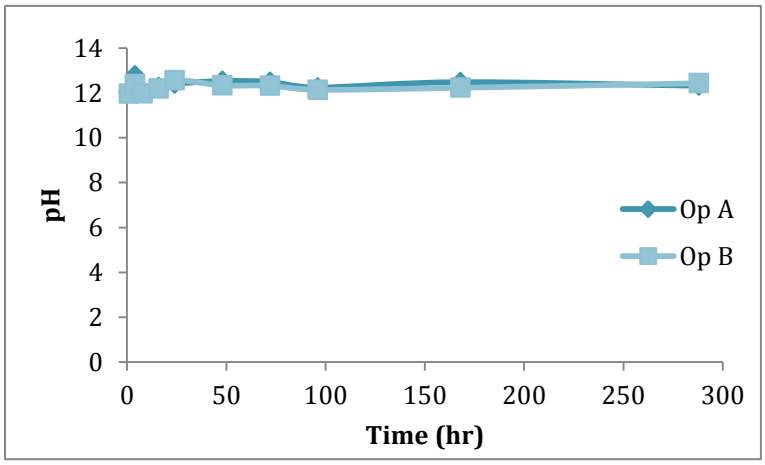

Figure 42. Water pH versus time for samples Op A and Op B

It is promising not to have significant iron leaching since it implies that the $ENP_{Fe\text{-}surf}$ added to the cementitious paste in the PCPC will remain within the matrix. No literature was found on leaching behavior of iron from cement paste in contact with deionized water. Bertron et al. (2005b) measured Fe concentration at 77 µmol/L (4.3 mg/L) after 10 hours from the specimens that had 50% of its Portland cement substituted by FA. However, their specimens were exposed to more aggressive environment (organic acid) and crushed prior to the exposure, which could have facilitated iron leaching.

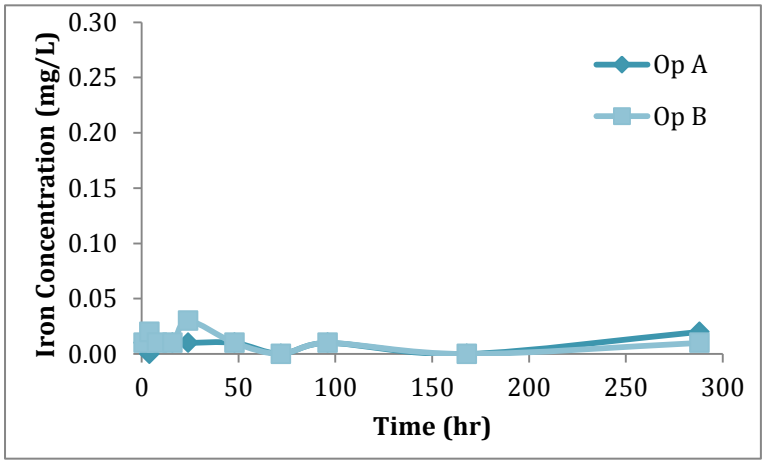

Figure 43. Iron concentrations in deionized water versus time for samples Op A and Op B

5.4 Phosphorus Removal by PCPC

5.4.1 Kinetic Study for Phosphorus Removal by PCPC

The phosphorus concentration (as PO_4^{3-}) in the solution was measured periodically throughout five days until the phosphorus concentration remained constant. The water pH after one hour was between 7.6 and 8.2 for all specimens. The water pH increased to around 12 after 24 hours and remained over 12 until the measurements ended. An example of the pH behavior is shown in Figure 44.

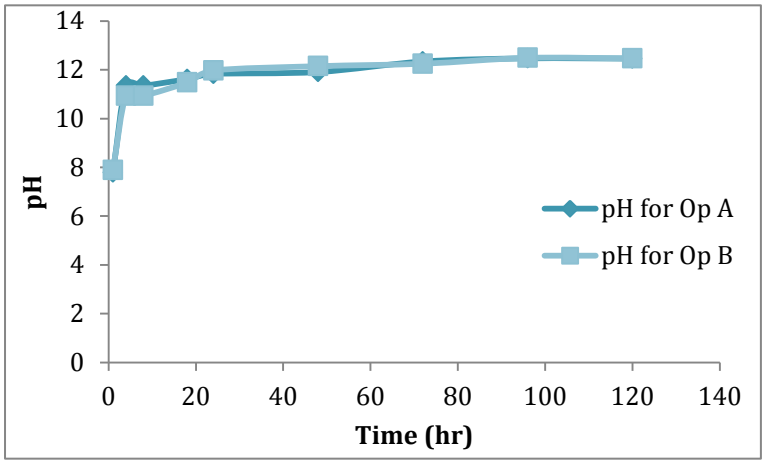

Figure 44. Water pH versus time for samples Op A and Op B

For all specimens the phosphorus concentration (as PO_4^{3-}) became constant after 72 hours (Figure 45-Figure 48). The phosphorus concentration had an exponential decrease for all four specimens. The highest R^2 value was obtained for sample C-3 (Figure 47) and the lowest was for sample C-2 (Figure 48), 0.97 and 0.95 respectively. Table 19 shows first-order phosphate removal constant for all four specimens. The PCPC specimens with $ENP_{Fe\text{-}surf}$ (C-3 and Op) had slightly higher values of removal constants. It is believed $ENP_{Fe\text{-}surf}$ presence contributes in the phosphate removal.

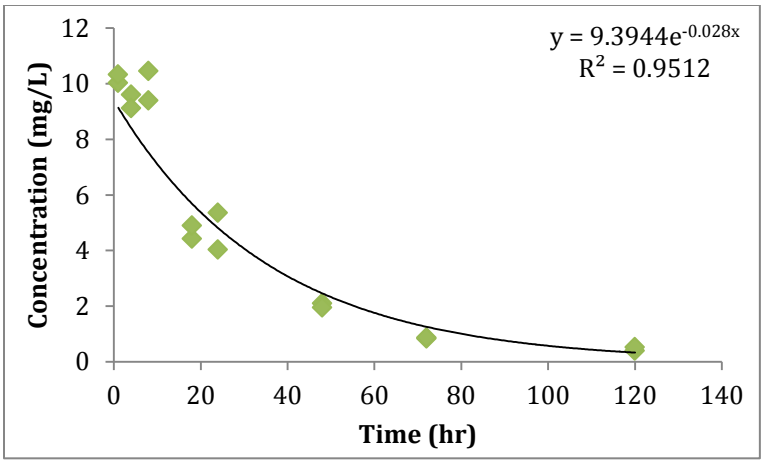

Figure 45. Phosphorus concentration (as PO_4^{3-}) versus time for sample C-1

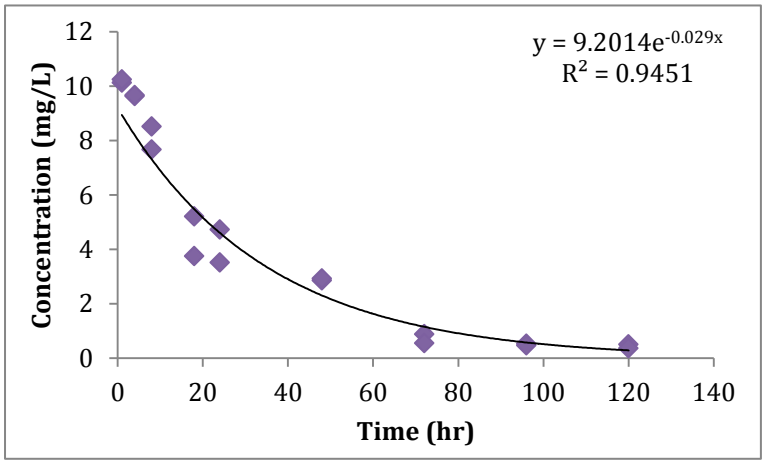

Figure 46. Phosphorus concentration (as PO_4^{3-}) versus time for sample C-2

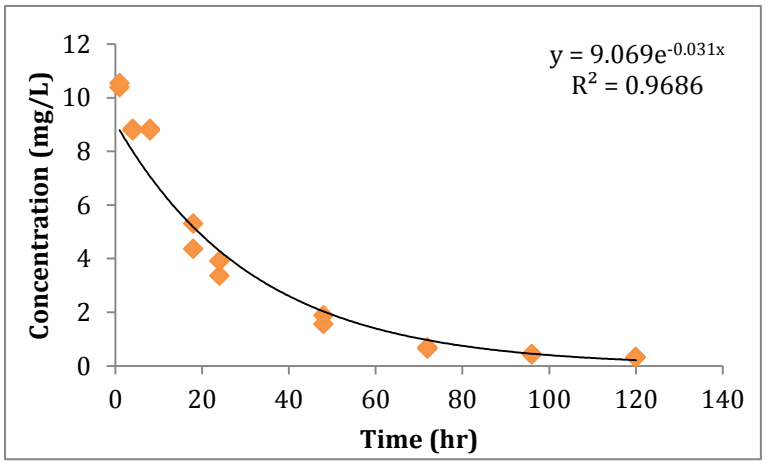

Figure 47. Phosphorus concentration (as PO_4^{3-}) versus time for sample C-3

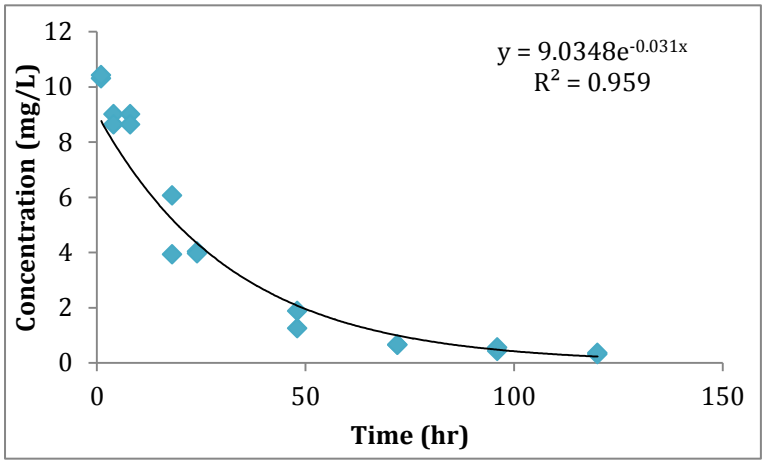

Figure 48. Phosphate concentration (as PO_4^{3-}) versus time for sample Op

Table 19. First-order phosphorus (as PO_4^{3-}) removal constants

Samples	First-order removal constant
C-1	0.028
C-2	0.029
C-3	0.031
Op	0.031

5.4.2 Removal Capacity of PCPC for Phosphorus

The specimens were also placed in phosphate solution with different concentrations until equilibrium time was reached (72 hours). The data obtained fits a Freundlich isotherm, as can be seen in Figure 49 to Figure 52. The C-3 PCPC specimen had the highest R^2 value (0.98) and C-2 the lowest (0.92). The Freundlich proportionality constant, K_f, and the slope, 1/n, are shown in Table 20 for each sample. The optimum PCPC specimens had a greater K_f value than the other PCPC specimens, meaning it has the highest adsorption capacity. The 1/n value of all specimens was larger than 1 meaning at low concentrations values the PCPC specimens are unfavorable for adsorption. Either way PCPC can still be utilized at the studied concentrations, further research

will be beneficial. It is believed that the combination of FA and $ENP_{Fe\text{-}surf}$ presence contributes to the phosphate removal by adsorption, although adsorption may not be the only method of removal.

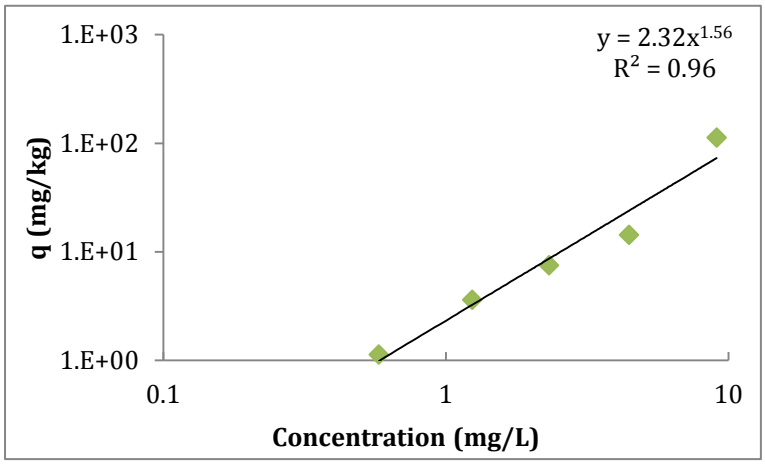

Figure 49. Freundlich isotherm for sample C-1

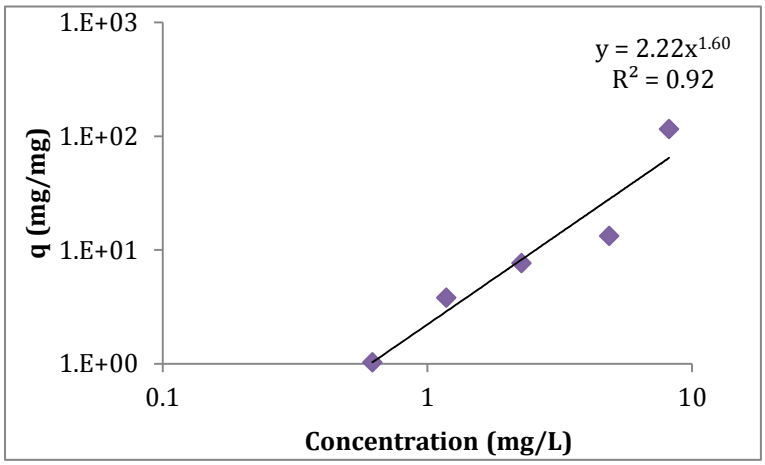

Figure 50. Freundlich isotherm for sample C-2

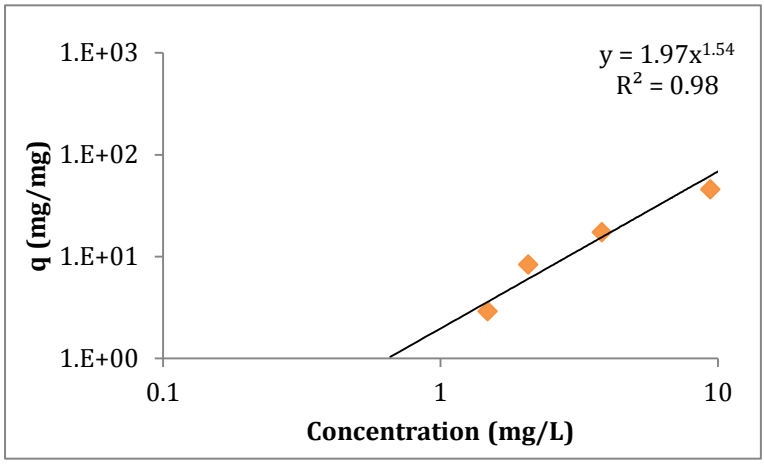

Figure 51. Freundlich isotherm for sample C-3

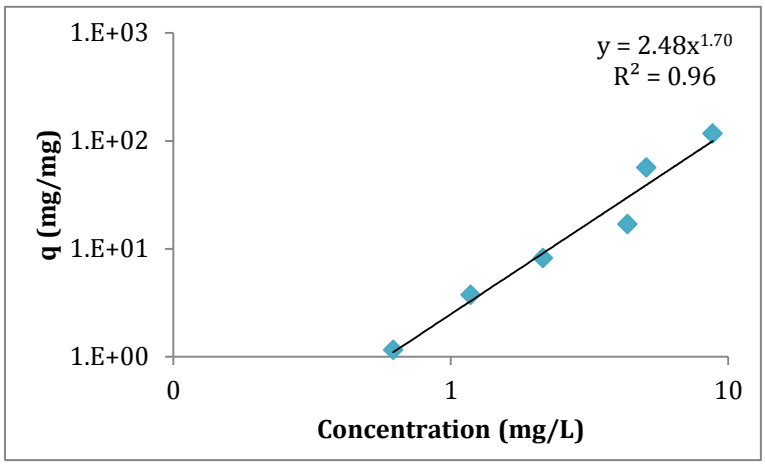

Figure 52. Freundlich isotherm for sample Op

Table 20. Freundlich isotherm values of each sample

Sample	K_f	1/n	R2
C1	2.32	1.56	0.96
C2	2.22	1.6	0.92
C3	1.97	1.54	0.98
OP	2.48	1.7	0.96

As the initial concentration of phosphate increased, more turbid the solution became with time as can be seen in Figure 53. Probably phosphate was removed by adsorption and co-precipitation with calcium ions. As phosphate ions available for co-precipitation increased more

$Ca(OH)_2$ dissolve creating more micro-pores within the cementitious paste of the PCPC specimen. By increasing the quantity micro-pores within the paste the PCPC will be debilitated. Regardless of phosphate removal mechanisms, either precipitation or adsorption, PCPC seemed to possess capacity to remove phosphate.

Figure 53. PCPC specimens after 72 hours exposed to a) 5mg/L, b) 10 mg/L, c)25 mg/L and d) 50 mg/L initial phosphate concentration

Park and Tia (2003) also studied PCPC's capacity to remove phosphorus from water, but attributed the removal to microorganisms growing within the pores. On the other hand, Luck et al. (2008) attributed the phosphorus removal to precipitation caused by the presence of Ca^{2+} or

Mg^{2+} ions that were leached from the PCPC cementitious matrix. There has been research on the precipitation of phosphate with Ca^{2+} ions provided by calcium hydroxide, xonolite, steel slag and amorphous calcium silicate hydrates (Chen et al., 2009; Okano et al., 2013). All of these authors proposed the formation of hydroxyapatite ($Ca_5(PO_4)_3OH$), which can be used in the production of fertilizers. Okano et al. (2013) and Chen et al. (2009) used amorphous calcium silicate hydrates and xonolite respectively; to precipitate phosphate, but both measured lower pH values. Both aforementioned researchers related the pH values between 7 and 8 to the consumption of both Ca^{2+} and OH^- ions, but in this research this particular pH behavior was not observed. In the current study, producing a complex such as hydroxyapatite might precipitate phosphate, but the pH was not decreased. This was believed to be attributed to high concentrations of $Ca(OH)_2$ that maintains the pH higher than 11. Hosni et al. (2008) found that calcium hydroxide at an initial Ca/P ratio and pH of 1.27 and 11, respectively, can precipitate phosphate as a mixture of phases that include hydroxyapatite ($Ca_{10}(PO_4)_6(OH)_2$) and amorphous calcium phosphate ($Ca_3(PO_4)_2$). Probably phosphate ions were precipitating as amorphous calcium phosphate and/or hydroxyapatite in the current study. Phosphorus is an element utilized in various industrial productions therefore phosphate recuperation is advantageous. A system can be designed in order to recover the precipitated calcium phosphate compounds in future studies.

5.5 PCPC Clogging and Fenton Oxidation

Figure 54 shows the pH behavior in the reservoir 1 with the PCPC specimens with the C-2 design (15% FA/B, 0% ENP/B), and in the reservoir 2 with the PCPC specimens with the optimum design (15% FA/B, 5% ENP/B). The pH of the creek water started above 11, but it gradually decreased. The pH reached 7 after the systems were bio-augmented with activated

sludge and remained at approximately 8. The reservoir with the C-2 specimens dropped pH more and earlier compared to the reservoir with the optimum design specimens. This phenomenon was probably attributed to more bacterial activity found in the reservoir with the C-2 specimens. The microorganisms might utilize more the added glucose and the other carbon sources in the reservoir with the C-2 specimens resulting in a greater decrease in pH and more bacterial activity.

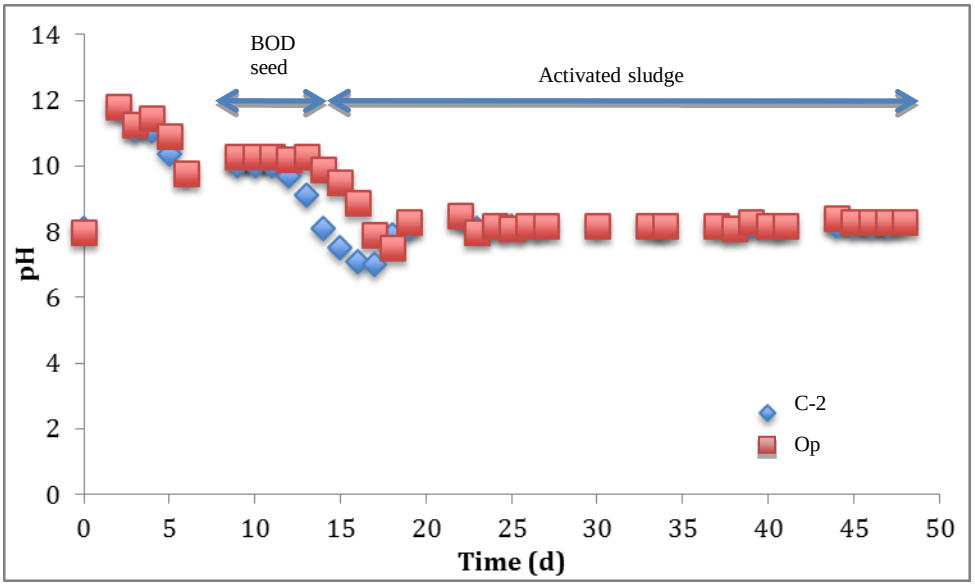

Figure 54. pH versus time (d) for reservoir 1 (specimens C-2 design) and reservoir 2 (specimens optimum design)

Figure 55 shows the surfaces, of PCPC specimens with C-2 and optimum design after the second bio-clogging stage. Visually, the specimens with the optimum design had more biofilm attachment on the surface than the ones with C-2 design.

Figure 55. PCPC specimens after second clogging a)top view of C-2 PCPC, b) side view of C-2 PCPC, c) top view of optimum PCPC and d) side view of optimum PCPC

Changes in permeability after each bio-clogging and Fenton regeneration are shown in Figure 56. It should be noted that the same specimens tested for permeability at each stage of bio-clogging and Fenton regeneration. It is also worthwhile to mention that the initial permeability of C-2 was higher (10.4 mm/s) than that of optimum design specimens (7.6 mm/s) and variability between specimen with the same design were observed. Variability in permeability among the specimens despite the same mixture design was also reported by Brovelli et al. (2009). In general, C-2 specimens had permeability reductions due to bio-clogging and showed increase in permeability after Fenton regeneration up the third time. After the 4th

and 5th Fenton regeneration there were no changes in the permeability. In comparison, neither bio-clogging nor Fenton regeneration modified the permeability of the optimum design specimens, except for the 2nd bio-clogging and Fenton regeneration. It is construed that this discrepancy in permeability change was due to the higher initial permeability of C-2 specimens compared to the optimum design specimens, and not due to the presence of $ENP_{Fe\text{-}surf}$ in optimum design specimens.

As described previously, iron species are essential to initiate Fenton reaction. Although C-2 specimens did not contain $ENP_{Fe\text{-}surf}$, Fenton reaction could be initiated with iron compounds present in FA. In fact, both C-2 and optimum design specimens contained 15% of FA and the FA consisted of 4.35% of Fe_2O_3 (Table 2).

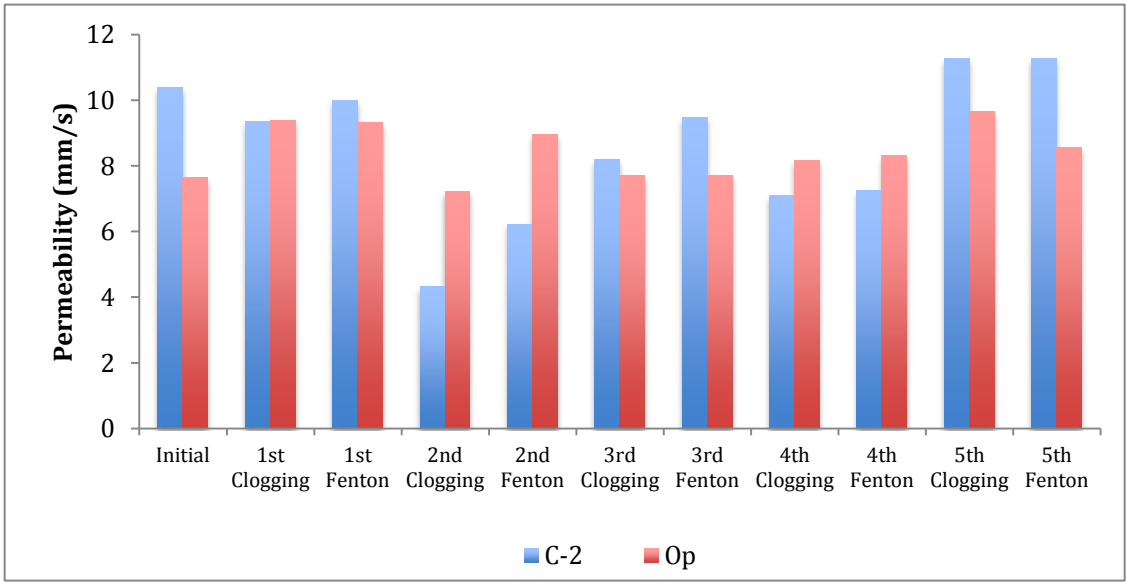

Figure 56. Permeability of PCPC with C-2 and optimum design

Potential effect of strong Fenton oxidation reaction on the structural strength of the specimens was tested after Fenton regeneration. As shown in Figure 68, the compressive strength

was generally increased up to the 3rd Fenton, but it decreased afterward. Although this decrease was observed, the compressive strength values are still in the range of observed values or close to it. It is believed that such an increase in compressive strength was attributed to the experimental setup where the specimens were submerged in the water for bio-clogging. The variation in compressive strength could be attributed to the variability in void content from one sample to another. Therefore, Fenton regeneration of bio-clogged PCPC would not negatively impact the compressive strength of PCPC.

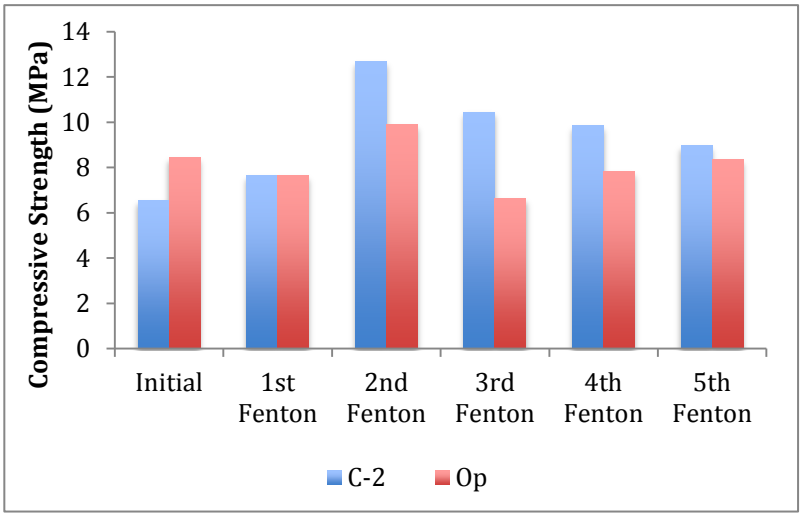

Figure 57. Compressive strength of PCPC with C-2 and optimum design

6. Conclusions

All the objectives of this research were achieved especially identifying the optimum design of PCPC. FA was utilized for partial substitution of Portland cement, leading to CO_2 reduction and solid waste beneficiation. $ENP_{Fe\text{-}surf}$ was added with the intention of facilitating the incorporation of FA into the cementitious matrix, to enhance durability and compressive strength, and utilize the nanoparticles as a catalyst in Fenton regeneration. The following specific conclusions were observed:

- The partial substitution of Portland cement by FA produced lower percentages of spread and setting time compared to cement only mixture. Furthermore the addition of $ENP_{Fe\text{-}surf}$ increased the percentage of spread and setting time even with the presence of FA.
- Iron leaching was not detected in deionized water and sodium chloride solutions. However, it was detected only in the presence of sulfuric acid in low concentrations below 0.08 mg/L.
- The $ENP_{Fe\text{-}surf}$ addition increased weight gain when exposed to sulfuric acid, and decreased weight loss when exposed to acetic acid.
- It is possible that $ENP_{Fe\text{-}surf}$ facilitated the production of C-S-H gel, iron-substituted monosulfate hydrate, or iron-substituted ettringite. The specimens exposed to sulfuric acid had higher compressive strength compared to those exposed to acetic acid for 90 days.
- The density (hardened concrete) of PCPC had an inverse Pearson correlation with regards to void content and permeability. The void content and permeability of PCPC had direct Pearson correlation. Although the compressive strength did not have a strong Pearson

correlation with the other responses, it had a weak direct correlation with the density and a weak inverse correlation with void content and permeability.

- The $ENP_{Fe\text{-}surf}$ only had a linear effect on the compressive strength and was part of the interactive effects for the permeability. Overlaid contour plots enabled the determination of the optimum PCPC design of 34% W/B, 15% FA/B and 5% ENP/B.
- The compressive strength of the optimized PCPC design did not reach the expected values after 7 days of curing. On the other hand, the PCPC specimens had void content, permeability and density values within the desired ranges. The PCPC specimens probably did not lose $ENP_{Fe\text{-}surf}$ since there were no detectable iron concentrations in the solutions.
- The phosphate concentration decreased exponentially through time in the presence of PCPC specimens. The presence of $ENP_{Fe\text{-}surf}$ facilitated phosphate removal, either by adsorption or precipitation, or both.
- Fenton regeneration of the bio-clogged PCPC specimens was possible even for the specimens without $ENP_{Fe\text{-}surf}$ addition probably due to the Fe_2O_3 in FA. In general, Fenton regeneration did not decrease compressive strength of the specimens.

Therefore, the addition of FA and $ENP_{Fe\text{-}surf}$ produced plausible effects on strength and durability of the PCPC. Water quality enhancement in terms of phosphorus reduction was also achieved by the addition of $ENP_{Fe\text{-}surf}$.

7. References

ACI, American Concrete Institute Committee 201. (2000). *Guide to Durable Concrete*. ACI 201.2R-01. American Concrete Institute, Michigan.

ACI, American Concrete Institute Committee 522. (2010) *Report on Pervious Concrete*. 1st Ed., ACI 522R-10. American Concrete Institute, Michigan.

Agyei, N.M., Strydom, C.A., Potgieter, J.H. (2002). The removal of phosphate ions from aqueous solution by fly ash, slag, ordinary Portland cement and related blends. Cement and Concrete Research, 32, 1889-1897.

Ahmaruzzaman, M. (2010). A review on the utilization of fly ash. Progress in Energy and Combustion Science, 36, 327-363.

Aziz, H.A., Othman, O.M., Amr, S.S.A. (2013). The performance of Electro-Fenton oxidation in the removal of coliform bacteria from landfill leachate. Waste Management, 33, 396-400.

Badawy, M.I., Ali, M.E.M. (2006). Fenton's peroxidation and coagulation processes for the treatment of combined industrial and domestic wastewater. Journal of Hazardous Materials, 136, 961-966.

Bertron, A., Duchesne, J., Escadeillas, G. (2005a). Accelerated tests of hardened cement pastes alteration by organic acids: analysis of the pH effect. Cement and Concrete Research, 35, 155-166.

Bertron, A., Duchesne, J., Escadeillas, G. (2005b). Attack of cement pastes exposed to organic acids in manure. Cement & Concrete Composites, 27, 898-909.

Brovelli, A., Malaguerra, F., Barry, D.A. (2009). Bioclogging in porous media: Model development and sensitivity to initial conditions. Environmental Modelling & Software, 24, 611-626.

Chang, Z., Song, X., Munn, R., Marosszeky M. (2005). Using limestone aggregates and different cements for enhancing resistance of concrete to sulfuric acid attack. Cement and Concrete Reseach, 35, 1486-1494.

Chapra, S.C. (1997). *Surface Water-Quality Modeling*, Waveland Press Inc., Illinois.

Chen, X., Kong, H., Wu, D., Wang, X., Lin, Y. (2009). Phosphate removal and recovery through crystallization of hydroxyapatite using xonotlite as seed crystal. Journal of Environmental Sciences, 21, 575-580.

Chen, Y., Wang, K., Wang, X., Zhou, W. (2013). Strength, fracture and fatigue of pervious concrete. Construction and Building Materials, 42, 97-104.

Chindaprasirt, P., Hatanaka, S., Chareerat, T., Mishima, N., Yuasa, Y. (2008). Cement paste characteristics and porous concrete properties. Construction and Building Materials, 22, 894-901.

Cho, I.-H., Zoh, K.-D. (2007). Photocatalytic degradation of azo dye (Reactive Red 120) in TiO_2/UV system: Optimization and modeling using a response surface methodology (RSM) based on the central composite design. Dyes and Pigments, 75, 533-543.

Chopra, M., Kakuturu, S., Ballock, C., Spence, J., Wanielista, M. (2010). Effect of rejuvenation methods on the infiltration rates of pervious concrete pavements. Journal of Hydrologic Engineering, 15, 426-433.

Daou, T.J., Begin-Colin, S., Grenèche, J.M., Thomas, F., Derory, A., Bernhardt, P., Legaré, P., Pourroy, G. (2007). Phosphate adsorption properties of magnetite-based nanoparticles. Chemistry of Materials, 19, 4494-4505.

Deschner, F., Winnefeld, F., Lothenbach, B., Seufert, S., Schwesig, P., Dittrich, S., Goetz-Neunhoeffer, F., Neubauer, J. (2012). Hydration of Portland cement with high replacement by siliceous fly ash. Cement and Concrete Research, 42, 1389-1400.

EIA. (2013). "Electricity in the US." United States Energy Information Administration, *h*ttp://www.eia.gov/energyexplained/index.cfm?page=electricity_in_the_united_states retrieved August 1, 2013.

EPA. (1999). *Preliminary Data Summary of Urban Storm Water Best Management Practices*. EPA-821-R-99-012. United States Environmental Protection Agency, Office of Water, Washington DC.

EPA. (2010). Puerto Rico Water Quality Standards Regulation. Office of the Governor. Environmental Quality Board. Commonwealth of Puerto Rico.

Fan, Y.F., Hu, Z.Q., Zhang, Y.Z., Liu, J.L. (2010). Deterioration of compressive property of concrete under simulated acid rain environment. Construction and Building Materials, 24, 1975-1983.

Garber, G. (2010). *Paving with Pervious Concrete*, Schiffer Publishing, Pennsylvania.

Gilbert, J.K., Clausen, J.C. (2006). Stormwater runoff quality and quantity from asphalt, paver and crushed stone driveways in Connecticut. Water Research, 40, 826-832.

Gruyaert, E., Van den Heede, P., Maes, M., De Belie, N. (2012). Investigation of the influence of blast-furnace slag on the resistance of concrete against organic acid or sulphate attack by means of accelerated degradation tests. Cement and Concrete Research, 42, 173-185.

Hosni, K., Ben Moussa, S., Chachi, A., Ben Amor, M. (2008). The removal of PO_4^{3-} by calcium hydroxide from synthetic wastewater: optimization of the operating conditions. Desalination, 223, 337-343.

Hossain, K.M.A., Lachemi, M. (2006). Performance of volcanic ash and pumice based blended cement concrete in mixed sulfate environment. Cement and Concrete Research, 36, 1123-1133.

Huang, B., Wu, H., Shu, X., Burdette, E.G. (2010). Laboratory evaluation of permeability and strength of polymer-modified pervious concrete. Construction and Building Materials, 24, 818-823.

Ivanov, V., Chu, J. (2008). Applications of microorganisms to geotechnical engineering for bioclogging and biocementation of soil in situ. Reviews in Environmental Science and Bio/Technology, 7, 139-153.

Ju-Nam, Y., Lead, J.R. (2008). Manufactured nanoparticles: An overview of their chemistry, interactions and potential environmental implications. Science of the Total Environment, 400, 396-414.

Kayhanian, M., Anderso, D., Harvey, J.T., Jones, D., Munhunthan, B. (2012). Permeability measurement and scan imaging to assess clogging of pervious concrete pavements in parking lots. Journal of Environmental Management, 95, 114-123.

Kim, L.H., Kayhanian, M., Zoh, K.D., Stenstrom, M.K. (2005). Modeling of highway stormwater runoff. Science of the Total Environment, 348, 1-18.

Kovler, K. (2012). Does the utilization of coal fly ash in concrete construction present a radiation hazard?. Construction and Building Materials, 29, 158-166.

Kunhanandan Nambiar, E.K., Ramamurthy K. (2006). Models relating mixture composition to the density and strength of foam concrete using response surface methodology. Cement & Concrete Composites, 28, 752-760.

Li, G. (2004). Properties of high-volume fly ash concrete incorporating nano-SiO_2. Cement and Concrete, 34, 1043-1049.

Luck, J.D., Workman, S.R., Coyne, M.S., Higgins, S.F. (2008). Solid material retention and nutrient reduction properties of pervious concrete mixtures. Biosystems Engineering, 100, 401-408.

Makhloufi, Z., Kadri, E.H. Bouhicha, M., Benaissa, A. (2012). Resistance of limestone mortars with quaternary binders to sulfuric acid solution. Construction and Building Materials, 26, 497-504.

Mehta P.K., Monteiro, P.J. (2013). *Concrete microstructure, properties, and materials*, McGraw Hill. 4th ed. New York.

Mehta, A., Prasad, G.S., Choudhury A.R. (2014). Cost effective production of pollulan from agri-industrial residues using response surface methodology. International Journal of Biological Macromolecules, 64, 252-256.

Mohammed B.S., Fang, O.C., Hossain, K.M.A., Lachemi, M. (2012). Mix proportioning of concrete containing paper mill residuals using response surface methodology. Construction and Building Materials, 35, 63-68.

Montgomery D.C. (2012) *Design and Analysis of Experiments*, John Wiley & Sons, Inc. 8th ed., Arizona.

Nieto-Juarez, J.I. (2012). Virus Inactivation by Homogeneous and Heterogeneous Fenton-like Processes. Ècole Polytechnique Fédérale de Lausanne, Thèse N° 5295.

Neyens, E., Baeyens, J. (2003). A review of classic Fenton's peroxidation as an advanced oxidation technique. Journal of Hazardous Materials, 98, 33-50.

Okano, K., Uemoto, M., Kagami, J., Miura, K., Aketo, T., Toda, M., Honda, K., Ohtake, H. (2013). Novel technique for phosphorus recovery from aqueous solutions using amorphous calcium silicate hydrates (A-CSHs). Water Research, 47, 2251-2259.

Oltulu, M., Sahin, R. (2013). Effect of nano-SiO_2, nano-Al_2O_3, nano-Fe_2O_3 powders on compressive strength and capillary water absorption of cement mortar containing fly ash: A comparative study. Energy and Buildings, 58, 292-301.

Pandey, V.C., Singh, N. (2010). Impact of fly ash incorporation in soil systems. Agriculture, Ecosystems and Environment, 136, 16-27.

Pando, M., Hwang, S. (2006). *Possible applications for circulating fluidized bed coal combustion by-products from the Guayama AES power plan.* Civil and Infrastructure Research Center, University of Puerto Rico at Mayaguez, Puerto Rico.

Park, S., Tia, M. (2004). An experimental study on the water-purification properties of porous concrete. Cement and Concrete Research, 34, 177-184.

Park, T.-J., Sambasivan, S., Fischer, D.A., Yoon, W.-S., Misewich, J.A. Wong, S.S. (2008). Electronic Structure and Chemstry of Iron-Based Metal Oxide Nanostructured Materials: A NEXAFS Investigation of $BiFeO_3$, $Bi_2Fe_4O_9$, α-Fe_2O_3, γ-Fe_2O_3, and Fe/Fe_3O_4. Journal of Physical Chemistry C, 112, 10359-10369.

Jiménez-Quero, V.G., León-Martínez, F.M., Montes-García, P., Gaona-Tiburcio, C., Chacón-Nava, J.G. (2013). Influence of sugar-cane bagasse ash and fly ash on the rheological behavior of cement pastes and mortars. Construction and Building Materials, 40, 691-701.

Rusevova, K., Kopinke, F.D., Georgi, A. (2012). Nano-size magnetic iron oxides as catalysts for heterogeneous Fenton-like reactions – Influence of Fe(II)/Fe(III) ratio on catalytic performance. Journal of Hazardous Materials, 241-242, 433-440.

Sanchez, F., Sobolev, K. (2010). Nanotecnology in concrete – A review. Construction and Building Materials, 24, 2060-2071.

Sansalone, J., Kuang, X., Ying, G., Ranieri, V. (2012). Filtration and clogging of permeable pavement loaded by urban drainage. Water Research, 46, 6763-6774.

Scholz, M., Grabowiecki, P. (2007). Review of permeable pavement systems. Building and Environment, 42, 3830-3836.

Sonebi, M., Bassouni, M.T. (2013). Investigating the effect of mixture design parameters on pervious concrete by statistical modeling. Construction and Building Materials, 38, 147-154.

Tang, S.C.N., Lo, I.M.C. (2013). Magnetic nanoparticles: Essential factors for sustainable environmental applications. Water Research, 47, 2613-2632.

Temuujin, J., Minjigmaa, A., Lee, M., Chen-Tan, N., van Riessen, A. (2011). Characteristics of class F fly ash geopolymer pastes immersed in acid and alkaline solutions. Cement and Concrete Composites, 33, 1086-1091.

UKY, University of Kentucky Center for Applied Energy Research. (2014). Coal Combustion By-Products (CCBs) How To…. Last updated January 14, 2014. <http://www.caer.uky.edu/kyasheducation/testing-mortar.shtml>

Wang, S., Wu, H. (2006). Environmental-benign utilization of fly ash as low-cost adsorbents. Journal of Hazardous Materials, 136, 482-501.

Xie, S., Qi, L., Zhou, D. (2004). Investigation of the effects of acid rain on the deterioration of cement concrete using accelerated test established in laboratory. Atmospheric Environment, 38, 4457-4466.

Xu, P., Zeng, G.M., Huang, D.L., Feng, C.L, Hu, S., Zhao, M.H., Lai, C., Wei, Z., Huang, C., Xie, G.X., Liu, Z.F. (2012). Use of iron oxide nanomaterials in wastewater treatment: A review. Science of Total Environment, 424, 1-10.

Yang, J., Jiang, G. (2003). Experimental study on properties of pervious concrete pavement materials. Cement and Concrete Research, 33, 381-386.

Yang, Y., He, Z., Wang, Y., Fan, J., Liang, Z., Stoffella, P.J. (2013). Dissolved organic matter in relation to nutrients (N and P) and heavy metals in surface runoff water as affected by temporal variation and land uses – A case study from Indian River Area, south Florida, USA. Agricultural Water Management, 118, 38-49.

Appendix

Appendix A. Response Surface Regression

Response Surface Regression: Compressive Strength (CompStrength) versus Block, W/P, FA/B, ENP/B

Estimated Regression Coefficients for CompStrength

Term	Coef	SE Coef	T	P
Constant	9.4669	0.4484	21.113	0.000
Block 1	0.6543	0.5770	1.134	0.268
Block 2	0.9443	0.5770	1.637	0.114
Block 3	-2.5478	0.5154	-4.943	0.000
Block 4	0.3393	0.5770	0.588	0.562
Block 5	1.9226	0.5770	3.332	0.003
W/P	1.1619	0.3023	3.844	0.001
FA/B	-2.0098	0.3023	-6.649	0.000
ENP/P	0.7027	0.3151	2.230	0.035
W/P*W/P	-0.4384	0.3031	-1.446	0.160
FA/B*FA/B	-0.1459	0.3031	-0.481	0.634
ENP/P*ENP/P	0.1051	0.3412	0.308	0.761
W/P*FA/B	0.4369	0.3902	1.120	0.274
W/P*ENP/P	-0.1744	0.3902	-0.447	0.659
FA/B*ENP/P	-0.2119	0.3902	-0.543	0.592

S = 1.56092 PRESS = 164.105
R-Sq = 81.09% R-Sq(pred) = 49.06% R-Sq(adj) = 70.50%

Analysis of Variance for CompStrength

Source	DF	Seq SS	Adj SS	Adj MS	F	P
Blocks	5	94.299	94.581	18.916	7.76	0.000
Regression	9	166.915	166.915	18.546	7.61	0.000
Linear	3	156.878	155.834	51.945	21.32	0.000
W/P	1	35.999	35.999	35.999	14.78	0.001
FA/B	1	107.719	107.719	107.719	44.21	0.000
ENP/P	1	13.160	12.116	12.116	4.97	0.035
Square	3	5.778	5.778	1.926	0.79	0.511
W/P*W/P	1	4.960	5.098	5.098	2.09	0.160
FA/B*FA/B	1	0.587	0.565	0.565	0.23	0.634
ENP/P*ENP/P	1	0.231	0.231	0.231	0.09	0.761
Interaction	3	4.259	4.259	1.420	0.58	0.632
W/P*FA/B	1	3.054	3.054	3.054	1.25	0.274
W/P*ENP/P	1	0.487	0.487	0.487	0.20	0.659
FA/B*ENP/P	1	0.718	0.718	0.718	0.29	0.592
Residual Error	25	60.912	60.912	2.436		
Lack-of-Fit	19	51.233	51.233	2.696	1.67	0.272
Pure Error	6	9.678	9.678	1.613		
Total	39	322.126				

Unusual Observations for CompStrength

Obs	StdOrder	CompStrength	Fit	SE Fit	Residual	St Resid
21	34	11.860	8.882	0.986	2.978	2.46 R
30	6	7.080	10.121	0.742	-3.041	-2.21 R
38	15	12.810	9.812	0.986	2.998	2.48 R

R denotes an observation with a large standardized residual.

Estimated Regression Coefficients for CompStrength using data in uncoded units

Term	Coef
Constant	-64.2036

Block 1 0.654293
Block 2 0.944293
Block 3 -2.54775
Block 4 0.339293
Block 5 1.92263
W/P 3.83675
FA/B -0.439578
ENP/P 1.44557
W/P*W/P -0.0487159
FA/B*FA/B -6.48647E-04
ENP/P*ENP/P 0.0262720
W/P*FA/B 0.00970833
W/P*ENP/P -0.0290625
FA/B*ENP/P -0.00706250

Predicted Response for New Design Points Using Model for CompStrength

Point	Fit	SE Fit	95% CI	95% PI
1	12.3056	1.08268	(10.0758, 14.5355)	(8.39325, 16.2180)
2	10.4112	0.74201	(8.8830, 11.9394)	(6.85169, 13.9707)
3	5.6581	1.09083	(3.4115, 7.9048)	(1.73616, 9.5801)
4	10.4112	0.74201	(8.8830, 11.9394)	(6.85169, 13.9707)
5	9.8372	1.08268	(7.6074, 12.0670)	(5.92482, 13.7496)
6	11.9266	1.09083	(9.6800, 14.1732)	(8.00459, 15.8486)
7	10.8156	1.08268	(8.5857, 13.0454)	(6.90316, 14.7279)
8	11.3895	0.74201	(9.8613, 12.9177)	(7.83003, 14.9490)
9	13.2840	1.08268	(11.0542, 15.5138)	(9.37159, 17.1964)
10	12.9049	1.09083	(10.6583, 15.1515)	(8.98293, 16.8269)
11	11.3895	0.74201	(9.8613, 12.9177)	(7.83003, 14.9490)
12	6.6365	1.09083	(4.3899, 8.8831)	(2.71449, 10.5585)
13	6.3835	1.08268	(4.1536, 8.6133)	(2.47107, 10.2959)
14	12.8019	1.08268	(10.5721, 15.0317)	(8.88951, 16.7143)
15	9.8062	0.74201	(8.2780, 11.3344)	(6.24669, 13.3657)
16	8.5994	1.09083	(6.3528, 10.8460)	(4.67741, 12.5214)
17	9.5228	1.09083	(7.2762, 11.7694)	(5.60084, 13.4448)
18	9.8062	0.74201	(8.2780, 11.3344)	(6.24669, 13.3657)
19	5.0876	0.98596	(3.0570, 7.1182)	(1.28524, 8.8900)
20	8.1542	0.65842	(6.7981, 9.5102)	(4.66509, 11.6432)
21	8.8823	0.98596	(6.8517, 10.9129)	(5.07992, 12.6847)
22	11.0470	0.98596	(9.0164, 13.0777)	(7.24465, 14.8494)
23	7.3900	0.91220	(5.5113, 9.2687)	(3.66652, 11.1135)
24	8.1542	0.65842	(6.7981, 9.5102)	(4.66509, 11.6432)
25	9.5818	1.01741	(7.4864, 11.6772)	(5.74447, 13.4192)
26	4.4829	0.98596	(2.4523, 6.5135)	(0.68051, 8.2853)
27	13.1169	1.08268	(10.8871, 15.3467)	(9.20451, 17.0293)
28	10.1212	0.74201	(8.5930, 11.6494)	(6.56169, 13.6807)
29	9.8378	1.09083	(7.5912, 12.0844)	(5.91584, 13.7598)
30	10.1212	0.74201	(8.5930, 11.6494)	(6.56169, 13.6807)
31	6.6985	1.08268	(4.4686, 8.9283)	(2.78607, 10.6109)
32	8.9144	1.09083	(6.6678, 11.1610)	(4.99241, 12.8364)
33	6.9192	0.65842	(5.5631, 8.2752)	(3.43009, 10.4082)
34	3.2479	0.98596	(1.2173, 5.2785)	(-0.55449, 7.0503)
35	3.8526	0.98596	(1.8220, 5.8832)	(0.05024, 7.6550)
36	6.9192	0.65842	(5.5631, 8.2752)	(3.43009, 10.4082)
37	6.1550	0.91220	(4.2763, 8.0337)	(2.43152, 9.8785)
38	9.8120	0.98596	(7.7814, 11.8427)	(6.00965, 13.6144)
39	8.3468	1.01741	(6.2514, 10.4422)	(4.50947, 12.1842)
40	7.6473	0.98596	(5.6167, 9.6779)	(3.84492, 11.4497)

Response Surface Regression: Permeability versus Block, W/P, FA/B, ENP/P

Estimated Regression Coefficients for Permeability

Term	Coef	SE Coef	T	P

Constant 8.9199 0.4893 18.228 0.000
Block 1 0.8408 0.6297 1.335 0.194
Block 2 -0.5425 0.6297 -0.862 0.397
Block 3 -0.3122 0.5625 -0.555 0.584
Block 4 -1.8242 0.6297 -2.897 0.008
Block 5 0.3841 0.6297 0.610 0.547
W/P -2.4537 0.3299 -7.438 0.000
FA/B 0.9290 0.3299 2.816 0.009
ENP/P -0.4094 0.3439 -1.191 0.245
W/P*W/P 0.9577 0.3308 2.895 0.008
FA/B*FA/B -0.1261 0.3308 -0.381 0.706
ENP/P*ENP/P -0.2376 0.3724 -0.638 0.529
W/P*FA/B -1.0706 0.4259 -2.514 0.019
W/P*ENP/P 0.9656 0.4259 2.267 0.032
FA/B*ENP/P -0.8956 0.4259 -2.103 0.046
S = 1.70350 PRESS = 176.409
R-Sq = 80.84% R-Sq(pred) = 53.41% R-Sq(adj) = 70.11%
Analysis of Variance for Permeability
Source DF Seq SS Adj SS Adj MS F P
Blocks 5 44.590 44.385 8.877 3.06 0.027
Regression 9 261.542 261.542 29.060 10.01 0.000
Linear 3 188.695 187.679 62.560 21.56 0.000
W/P 1 160.551 160.551 160.551 55.33 0.000
FA/B 1 23.015 23.015 23.015 7.93 0.009
ENP/P 1 5.130 4.114 4.114 1.42 0.245
Square 3 26.754 26.754 8.918 3.07 0.046
W/P*W/P 1 25.192 24.320 24.320 8.38 0.008
FA/B*FA/B 1 0.380 0.422 0.422 0.15 0.706
ENP/P*ENP/P 1 1.182 1.182 1.182 0.41 0.529
Interaction 3 46.093 46.093 15.364 5.29 0.006
W/P*FA/B 1 18.340 18.340 18.340 6.32 0.019
W/P*ENP/P 1 14.919 14.919 14.919 5.14 0.032
FA/B*ENP/P 1 12.834 12.834 12.834 4.42 0.046
Residual Error 25 72.548 72.548 2.902
Lack-of-Fit 19 47.914 47.914 2.522 0.61 0.806
Pure Error 6 24.634 24.634 4.106
Total 39 378.679
Unusual Observations for Permeability
Obs StdOrder Permeability Fit SE Fit Residual St Resid
27 3 12.090 9.494 1.182 2.596 2.12 R
28 5 5.980 9.761 0.810 -3.781 -2.52 R
R denotes an observation with a large standardized residual.
Estimated Regression Coefficients for Permeability using data in uncoded units
Term Coef
Constant 176.651
Block 1 0.840795
Block 2 -0.542538
Block 3 -0.312215
Block 4 -1.82421
Block 5 0.384128
W/P -8.57997
FA/B 1.05981
ENP/P -5.05660
W/P*W/P 0.106406
FA/B*FA/B -5.60382E-04
ENP/P*ENP/P -0.0594075
W/P*FA/B -0.0237917
W/P*ENP/P 0.160938
FA/B*ENP/P -0.0298542
Predicted Response for New Design Points Using Model for Permeability
Point Fit SE Fit 95% CI 95% PI
1 8.9460 1.18158 (6.5124, 11.3795) (4.6762, 13.2157)

2	8.3774	0.80979	(6.7096, 10.0452)	(4.4927, 12.2620)
3	15.6953	1.19048	(13.2435, 18.1472)	(11.4151, 19.9756)
4	8.3774	0.80979	(6.7096, 10.0452)	(4.4927, 12.2620)
5	6.0366	1.18158	(3.6030, 8.4701)	(1.7668, 10.3063)
6	5.2074	1.19048	(2.7556, 7.6593)	(0.9272, 9.4877)
7	6.9632	1.18158	(4.5297, 9.3967)	(2.6934, 11.2330)
8	9.3040	0.80979	(7.6363, 10.9718)	(5.4194, 13.1887)
9	9.8726	1.18158	(7.4391, 12.3061)	(5.6028, 14.1424)
10	6.1341	1.19048	(3.6823, 8.5859)	(1.8538, 10.4143)
11	9.3040	0.80979	(7.6363, 10.9718)	(5.4194, 13.1887)
12	16.6220	1.19048	(14.1702, 19.0738)	(12.3417, 20.9022)
13	9.8723	1.18158	(7.4388, 12.3058)	(5.6025, 14.1421)
14	6.8294	1.18158	(4.3959, 9.2629)	(2.5596, 11.0992)
15	7.0957	0.80979	(5.4279, 8.7635)	(3.2110, 10.9804)
16	5.4338	1.19048	(2.9819, 7.8856)	(1.1535, 9.7140)
17	8.6232	1.19048	(6.1713, 11.0750)	(4.3429, 12.9034)
18	7.0957	0.80979	(5.4279, 8.7635)	(3.2110, 10.9804)
19	16.9346	1.07602	(14.7185, 19.1507)	(12.7849, 21.0843)
20	10.3739	0.71857	(8.8940, 11.8539)	(6.5662, 14.1817)
21	8.9208	1.07602	(6.7047, 11.1369)	(4.7711, 13.0705)
22	8.5207	1.07602	(6.3045, 10.7368)	(4.3709, 12.6704)
23	10.4896	0.99552	(8.4393, 12.5399)	(6.4260, 14.5532)
24	10.3739	0.71857	(8.8940, 11.8539)	(6.5662, 14.1817)
25	9.0717	1.11035	(6.7849, 11.3585)	(4.8838, 13.2596)
26	11.5548	1.07602	(9.3387, 13.7709)	(7.4051, 15.7045)
27	9.4944	1.18158	(7.0609, 11.9279)	(5.2246, 13.7642)
28	9.7607	0.80979	(8.0929, 11.4285)	(5.8760, 13.6454)
29	11.2882	1.19048	(8.8363, 13.7400)	(7.0079, 15.5684)
30	9.7607	0.80979	(8.0929, 11.4285)	(5.8760, 13.6454)
31	12.5373	1.18158	(10.1038, 14.9708)	(8.2675, 16.8071)
32	8.0988	1.19048	(5.6469, 10.5506)	(3.8185, 12.3790)
33	8.6077	0.71857	(7.1278, 10.0876)	(4.7999, 12.4155)
34	9.7885	1.07602	(7.5724, 12.0046)	(5.6388, 13.9382)
35	15.1684	1.07602	(12.9522, 17.3845)	(11.0186, 19.3181)
36	8.6077	0.71857	(7.1278, 10.0876)	(4.7999, 12.4155)
37	8.7233	0.99552	(6.6730, 10.7737)	(4.6597, 12.7869)
38	6.7544	1.07602	(4.5383, 8.9705)	(2.6047, 10.9041)
39	7.3054	1.11035	(5.0186, 9.5922)	(3.1175, 11.4933)
40	7.1546	1.07602	(4.9385, 9.3707)	(3.0048, 11.3043)

Response Surface Regression: Void Content versus Block, W/P, FA/B, ENP/P

Estimated Regression Coefficients for Void Content

Term	Coef	SE Coef	T	P
Constant	14.9434	0.4402	33.947	0.000
Block 1	0.4879	0.5665	0.861	0.397
Block 2	-0.8955	0.5665	-1.581	0.126
Block 3	-1.0716	0.5060	-2.118	0.044
Block 4	-0.0455	0.5665	-0.080	0.937
Block 5	0.3212	0.5665	0.567	0.576
W/P	-2.3131	0.2968	-7.795	0.000
FA/B	0.8534	0.2968	2.876	0.008
ENP/P	-0.4779	0.3093	-1.545	0.135
W/P*W/P	0.7576	0.2976	2.546	0.017
FA/B*FA/B	-0.2080	0.2976	-0.699	0.491
ENP/P*ENP/P	-0.5466	0.3350	-1.632	0.115
W/P*FA/B	-0.6250	0.3831	-1.631	0.115
W/P*ENP/P	0.3500	0.3831	0.914	0.370
FA/B*ENP/P	-0.5500	0.3831	-1.436	0.164

S = 1.53242 PRESS = 157.363
R-Sq = 79.97% R-Sq(pred) = 46.30% R-Sq(adj) = 68.75%

Analysis of Variance for Void Content

Source	DF	Seq SS	Adj SS	Adj MS	F	P
Blocks	5	27.729	27.640	5.528	2.35	0.070
Regression	9	206.631	206.631	22.959	9.78	0.000
Linear	3	169.896	167.710	55.903	23.81	0.000
W/P	1	142.683	142.683	142.683	60.76	0.000
FA/B	1	19.421	19.421	19.421	8.27	0.008
ENP/P	1	7.791	5.605	5.605	2.39	0.135
Square	3	23.685	23.685	7.895	3.36	0.035
W/P*W/P	1	16.439	15.222	15.222	6.48	0.017
FA/B*FA/B	1	0.992	1.147	1.147	0.49	0.491
ENP/P*ENP/P	1	6.254	6.254	6.254	2.66	0.115
Interaction	3	13.050	13.050	4.350	1.85	0.164
W/P*FA/B	1	6.250	6.250	6.250	2.66	0.115
W/P*ENP/P	1	1.960	1.960	1.960	0.83	0.370
FA/B*ENP/P	1	4.840	4.840	4.840	2.06	0.164
Residual Error	25	58.708	58.708	2.348		
Lack-of-Fit	19	52.338	52.338	2.755	2.59	0.121
Pure Error	6	6.370	6.370	1.062		
Total	39	293.068				

Unusual Observations for Void Content

Obs	StdOrder	VoidContent	Fit	SE Fit	Residual	St Resid
27	3	15.900	13.315	1.063	2.585	2.34 R

R denotes an observation with a large standardized residual.

Estimated Regression Coefficients for Void Content using data in uncoded units

Term	Coef
Constant	148.457
Block 1	0.487879
Block 2	-0.895454
Block 3	-1.07159
Block 4	-0.0454541
Block 5	0.321213
W/P	-6.82830
FA/B	0.672000
ENP/P	-1.11898
W/P*W/P	0.0841821
FA/B*FA/B	-9.24346E-04
ENP/P*ENP/P	-0.136662
W/P*FA/B	-0.0138889
W/P*ENP/P	0.0583333
FA/B*ENP/P	-0.0183333

Predicted Response for New Design Points Using Model for Void Content

Point	Fit	SE Fit	95% CI	95% PI
1	14.6078	1.06292	(12.4187, 16.7969)	(10.7668, 18.4488)
2	14.0480	0.72846	(12.5477, 15.5483)	(10.5535, 17.5425)
3	19.2205	1.07092	(17.0149, 21.4261)	(15.3701, 23.0709)
4	14.0480	0.72846	(12.5477, 15.5483)	(10.5535, 17.5425)
5	11.2884	1.06292	(9.0992, 13.4775)	(7.4474, 15.1293)
6	11.0874	1.07092	(8.8818, 13.2930)	(7.2370, 14.9378)
7	12.5050	1.06292	(10.3159, 14.6941)	(8.6640, 16.3460)
8	15.2647	0.72846	(13.7644, 16.7650)	(11.7701, 18.7592)
9	15.8245	1.06292	(13.6354, 18.0136)	(11.9835, 19.6655)
10	12.3040	1.07092	(10.0984, 14.5096)	(8.4536, 16.1544)
11	15.2647	0.72846	(13.7644, 16.7650)	(11.7701, 18.7592)
12	20.4371	1.07092	(18.2315, 22.6427)	(16.5867, 24.2875)
13	17.3146	1.06292	(15.1255, 19.5038)	(13.4737, 21.1556)
14	12.7815	1.06292	(10.5924, 14.9707)	(8.9406, 16.6225)
15	14.8980	0.72846	(13.3977, 16.3983)	(11.4035, 18.3925)
16	13.4942	1.07092	(11.2886, 15.6998)	(9.6438, 17.3446)
17	16.0136	1.07092	(13.8080, 18.2192)	(12.1633, 19.8640)

18	14.8980	0.72846	(13.3977, 16.3983)	(11.4035, 18.3925)
19	21.9446	0.96796	(19.9510, 23.9381)	(18.2116, 25.6776)
20	16.1469	0.64640	(14.8156, 17.4781)	(12.7215, 19.5722)
21	14.3899	0.96796	(12.3963, 16.3834)	(10.6569, 18.1229)
22	14.1986	0.96796	(12.2051, 16.1922)	(10.4657, 17.9316)
23	15.7786	0.89554	(13.9342, 17.6231)	(12.1231, 19.4341)
24	16.1469	0.64640	(14.8156, 17.4781)	(12.7215, 19.5722)
25	13.9087	0.99884	(11.8515, 15.9658)	(10.1414, 17.6760)
26	16.9859	0.96796	(14.9923, 18.9794)	(13.2529, 20.7188)
27	13.3149	1.06292	(11.1258, 15.5040)	(9.4739, 17.1559)
28	15.4313	0.72846	(13.9310, 16.9316)	(11.9368, 18.9259)
29	16.5470	1.07092	(14.3414, 18.7526)	(12.6966, 20.3974)
30	15.4313	0.72846	(13.9310, 16.9316)	(11.9368, 18.9259)
31	17.8480	1.06292	(15.6589, 20.0371)	(14.0070, 21.6889)
32	14.0275	1.07092	(11.8219, 16.2331)	(10.1771, 17.8779)
33	13.8719	0.64640	(12.5406, 15.2031)	(10.4465, 17.2972)
34	14.7109	0.96796	(12.7173, 16.7044)	(10.9779, 18.4438)
35	19.6696	0.96796	(17.6760, 21.6631)	(15.9366, 23.4026)
36	13.8719	0.64640	(12.5406, 15.2031)	(10.4465, 17.2972)
37	13.5036	0.89554	(11.6592, 15.3481)	(9.8481, 17.1591)
38	11.9236	0.96796	(9.9301, 13.9172)	(8.1907, 15.6566)
39	11.6337	0.99884	(9.5765, 13.6908)	(7.8664, 15.4010)
40	12.1149	0.96796	(10.1213, 14.1084)	(8.3819, 15.8479)

Appendix B. Normality, Equal Variance and Independence Test

Test for Normality:

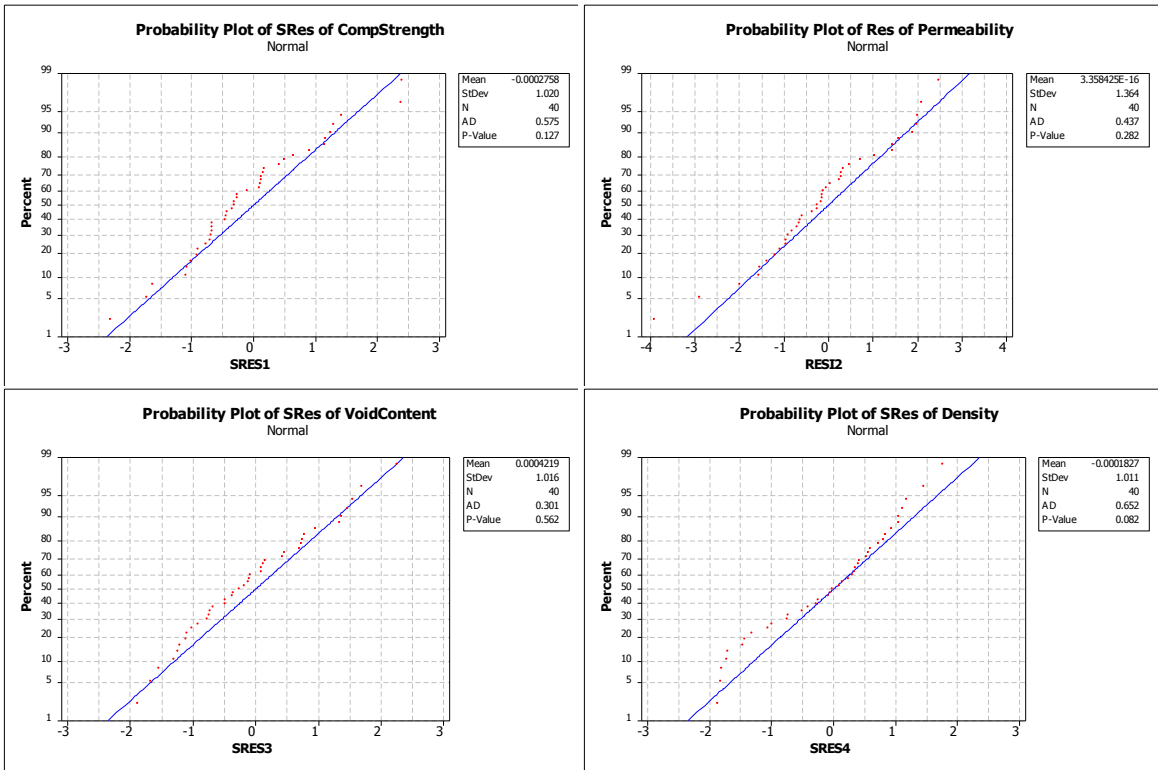

Figure 58 Normality Test for each response

Test for Equal Variance:

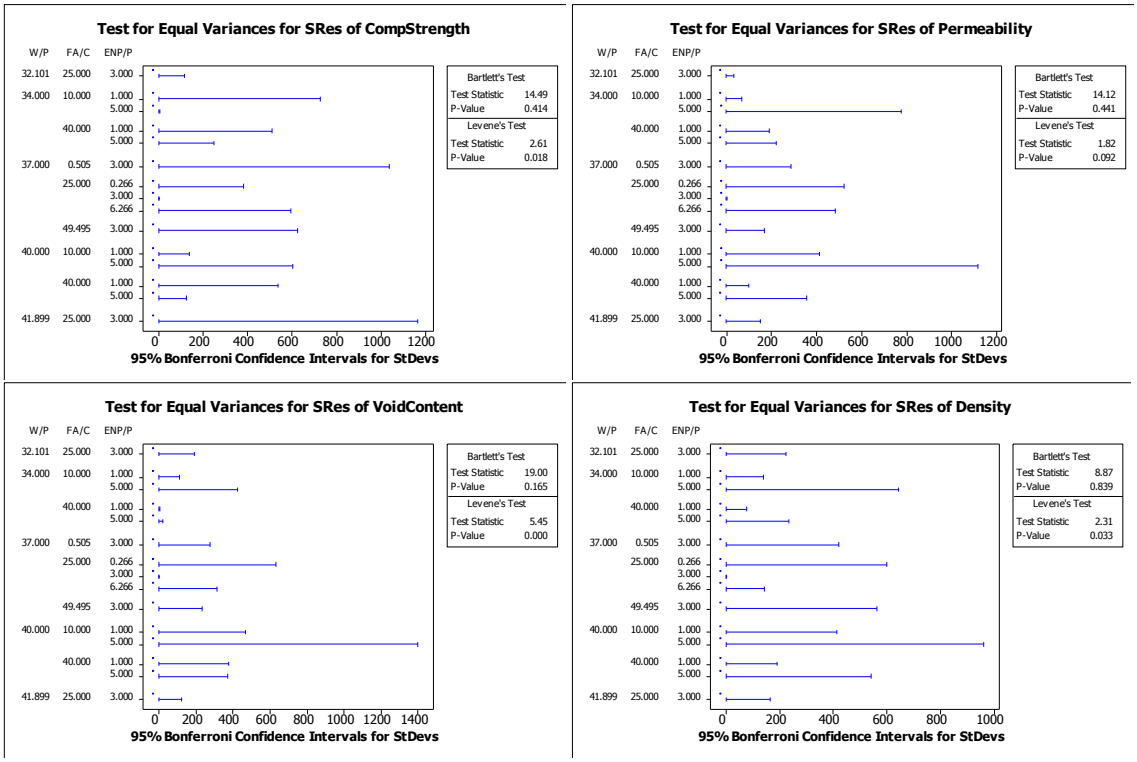

Figure 59 Equal Variance Test for each response

Test for Independence:

Compressive Strength:

```
Runs test for SRECS
Runs above and below K = -0.000275843
The observed number of runs = 23
The expected number of runs = 20.55
17 observations above K, 23 below
P-value = 0.422
```

Permeability:

```
Runs test for SREP
Runs above and below K = 0.00102078
The observed number of runs = 21
The expected number of runs = 20.55
17 observations above K, 23 below
P-value = 0.883
```

Void Content:

```
Runs test for SREVC
Runs above and below K = 0.000421950
The observed number of runs = 20
The expected number of runs = 20.8
18 observations above K, 22 below
P-value = 0.796
```

Density:

```
Runs test for SREHD
Runs above and below K = -0.000182677
The observed number of runs = 19
The expected number of runs = 20.2
24 observations above K, 16 below
P-value = 0.688
```

Appendix C. Surface and Contour Plots from RSM

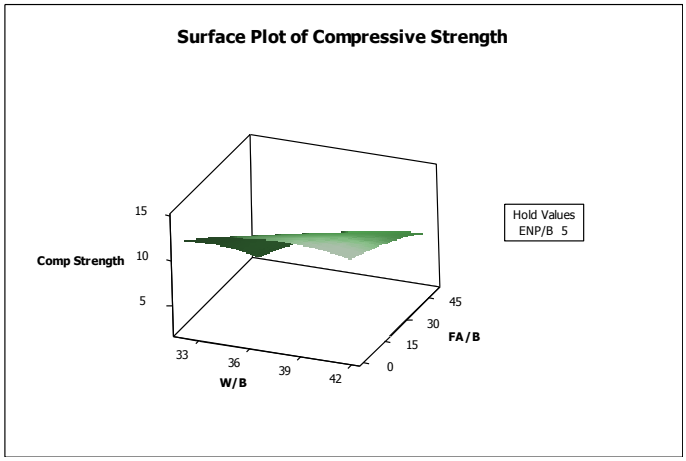

Figure 60 Surface Plot of Compressive Strength versus W/B and FA/B with ENP/B constant at 5%

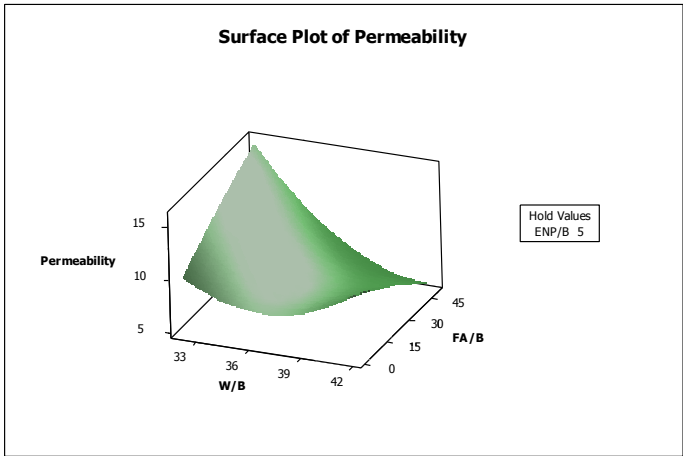

Figure 61 Surface Plot of Permeability versus W/B and FA/B with ENP/B constant at 5%

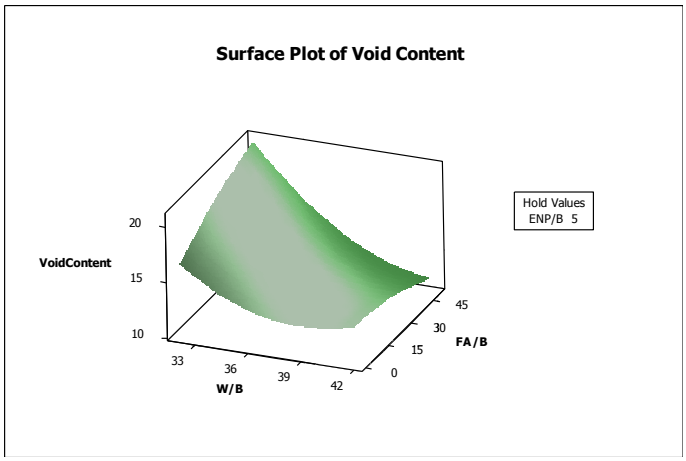

Figure 62 Surface Plot of Void Content versus W/B and FA/B with ENP/B constant at 5%

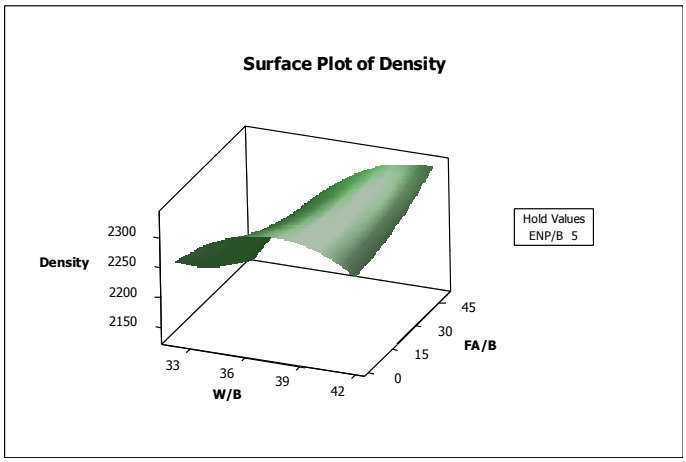

Figure 63 Surface Plot of Density of Hardened Concrete versus W/P and FA/B with ENP/B constant at 5%

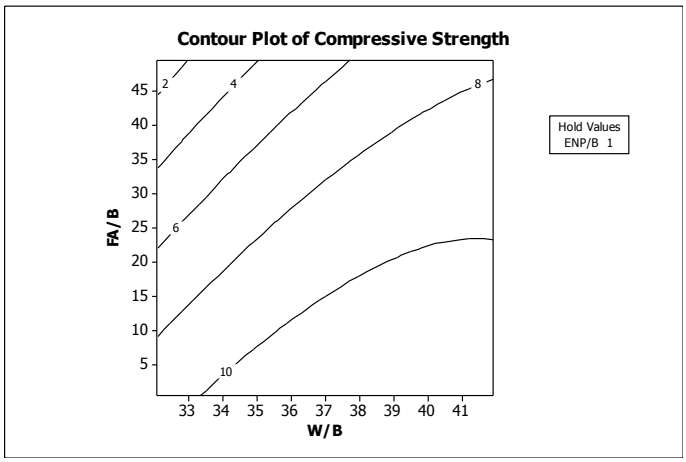

Figure 64 Contour Plot of Compressive Strength versus W/B and FA/B with ENP/B constant at 1%

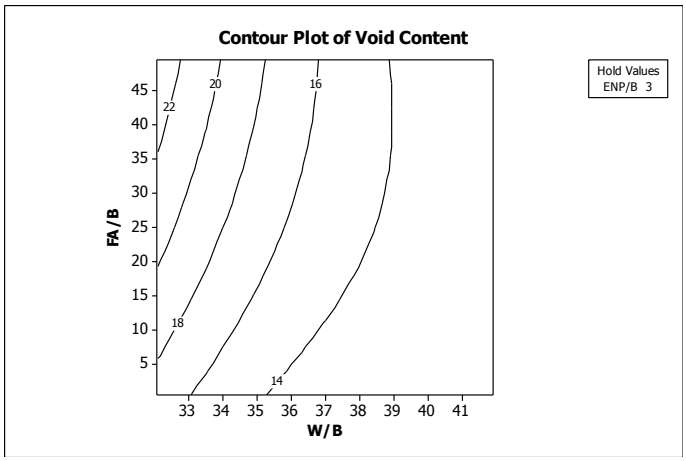

Figure 65 Contour Plot of Void Content versus W/B and FA/B with ENP/B constant at 3%

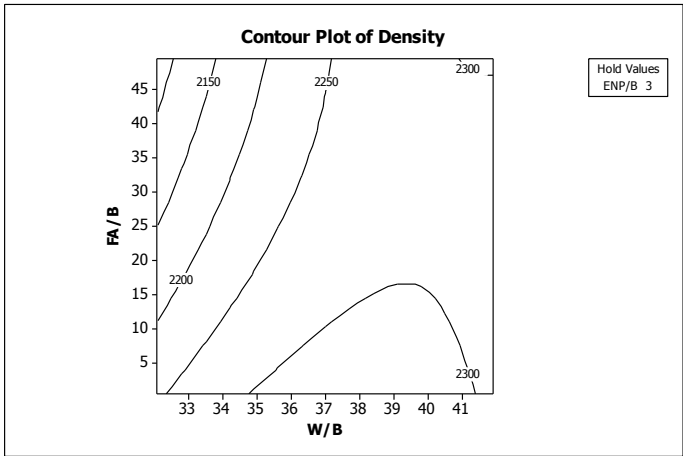

Figure 66 Contour Plot of Density versus W/B and FA/B with ENP/B constant at 3%

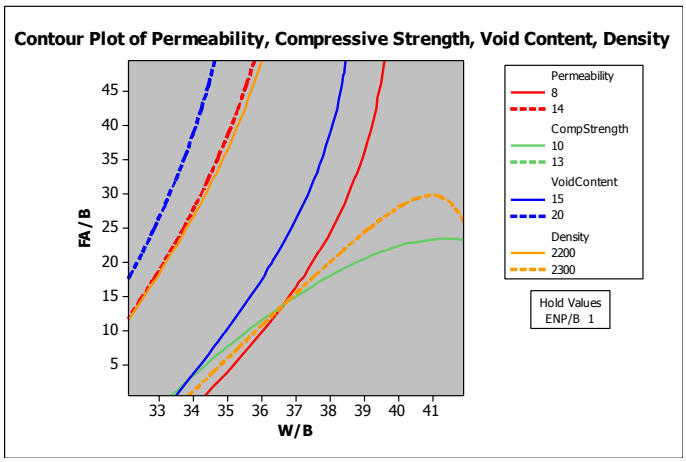

Figure 67 Overlaid Contour Plot of all responses versus W/B and FA/B with ENP/B constant at 3%

Appendix D Optimum and control specimens results

Iron leaching results:

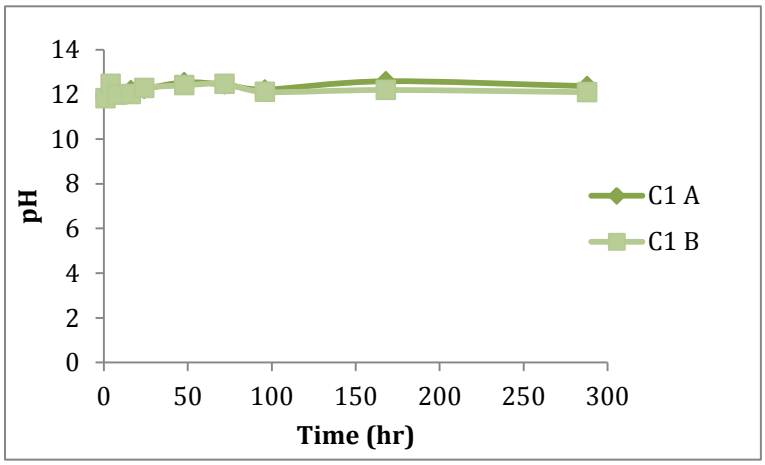

Figure 68 Water pH versus time for samples C-1 A and C-1 B

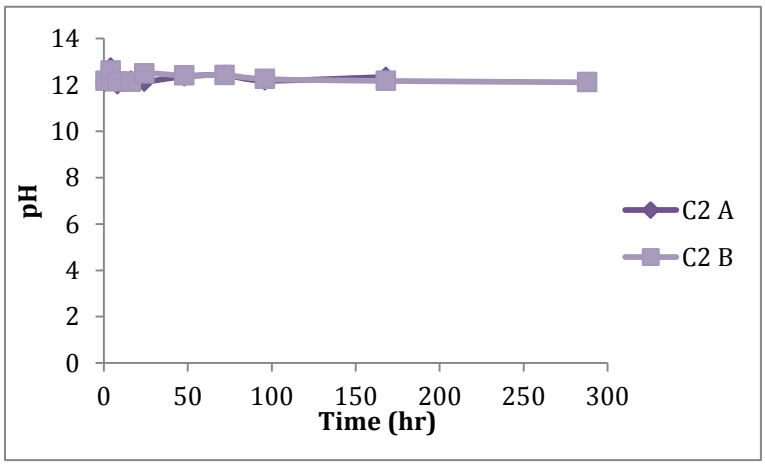

Figure 69 Water pH versus time for samples C-2 A and C-2 B

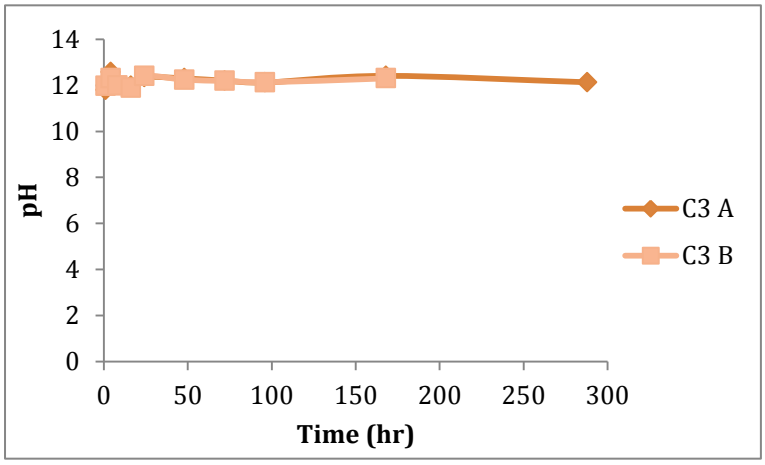

Figure 70 Water pH versus time for samples C-3 A and C-3 B

Kinetic study of phosphate removal:

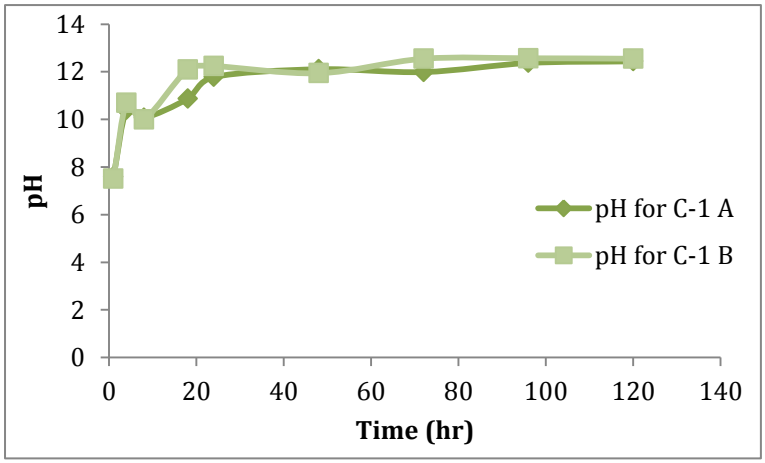

Figure 71 pH versus time for samples C-1 A and C-1 B

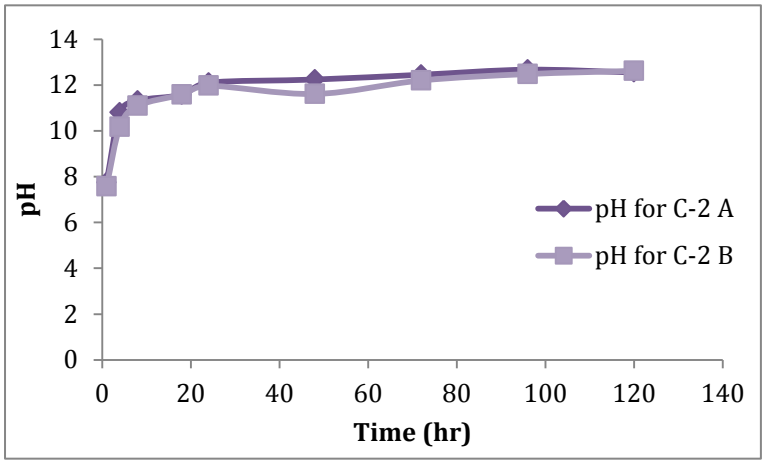

Figure 72 Water pH versus time for samples C-2 A and C-2 B

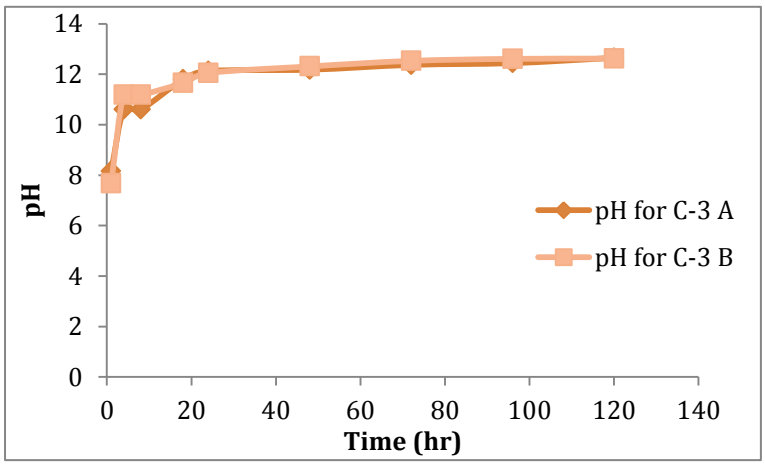

Figure 73 Water pH versus time for samples C3 A and C3 B